Chapter Five

In-situ Neutron-beam Diffraction Studies of the Palladium-Deuterium System:

Deuterium Occupation of the Tetrahedral Site

Chapter Five

In-situ Neutron-beam Diffraction Studies of the Palladium-Deuterium System:

Deuterium Occupation of the Tetrahedral Site

5.1 Introduction

When forming palladium-hydrogen there are two sites in the face centered cubic (FCC) palladium crystal structure that a hydrogen atom could possibly occupy. These are the octahedral site and the tetrahedral site, and are illustrated in Fig 5 1

To illustrate using palladium, the tetrahedral site lies at the center of a tetrahedron formed by a corner palladium atom and the three nearest face-centered palladium atoms There are eight equivalent tetrahedral sites in the cube The octahedral site lies in the center of the octahedron formed by the six face-centered palladium atoms. There are four equivalent octahedral sites.

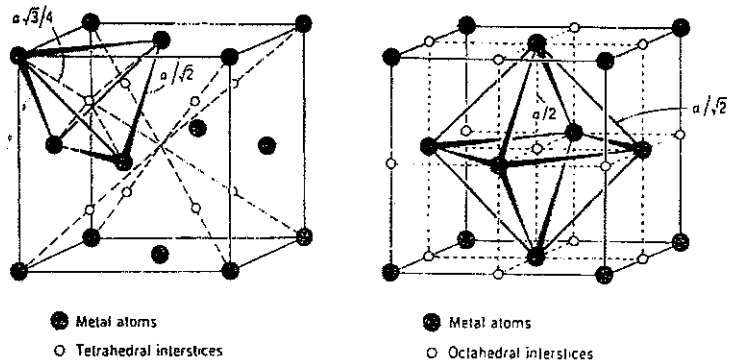

Fig 5 1: Location of the tetrahedral and octahedral sites in the face centered cubic structure [1]

Neutron-beam diffraction studies of palladium-deuterium have generally concluded that the deuterium atoms, and by extension hydrogen atoms, occupy the octahedral position of the FCC palladium structure. The study which prompted the research in the current chapter is presented in [2] and Chapter 7 of [3], and presents compelling evidence for deuterium occupying some tetrahedral positions. A short history of diffraction studies of

the palladium-hydrogen system, specific to the question of octahedral versus tetrahedral occupation, follows.

Firstly, X-ray diffraction studies do not reveal details of hydrogen positions. The very earliest experiments did show that neither α or β phases diverge from the pure palladium FCC structure [4], at least as far as the metal sub-structure is concerned. X-rays also revealed the single phase nature of palladium hydride above the thermodynamic critical point [5]

The first neutron diffraction experiment [6], which studied $PdH_{0.71}$ and $PdD_{0.66}$, concluded that the both hydrogen and deuterium atoms occupied octahedral positions only. The first single crystal neutron diffraction study [7] did not consider tetrahedral occupation in the $PdH_{0.63}$ sample, but did confirm that the method of loading the hydrogen, from the gaseous phase or electrochemically, produced no structural differences. This was also confirmed in [8] and [9]

The two studies [6] and [7] also showed that the structure of β-phase palladium-hydrogen and β-phase palladium-deuterium is of the NaCl type (i.e two interlocked FCC lattices) with the hydrogen atoms occupying random positions, regardless of whether the hydrogen is loaded electrochemically or from the gas phase.

The observation of an anomalous heat capacity in β-phase palladium-hydride [10] has spawned many micro-structural investigations using both neutrons [11-26] and X-rays [27] This anomaly has now been attributed to an ordered deuterium super-lattice with a $MoNi_4$ structure in the space group $Pm\bar{3}n$. Of these studies [11] proposed a phase transition that involved migration of hydrogen or deuterium from octahedral to tetrahedral sites in space group $R\bar{3}m$, though this model was dismissed in an early review by Jacobs *et al* [28].

Before the experiments conducted for the current thesis on MRPD at HIFAR ANSTO in October 2001, the only successful neutron diffraction study of super-critical temperature palladium deuteride was carried out by Nelin [29], who looked at β-$PdH_{0.75}$, α-$PdD_{0.10}$, α-$PdH_{0.09}$ and α-$PdH_{0.13}$ from room temperature up to 320°C. The possibility of tetrahedral occupation is inconclusive in Nelin's study due to poor data.

The studies mentioned so far, if they have considered tetrahedral occupation at all, have considered pure octahedral or pure tetrahedral occupation only, and not mixed octahedral+tetrahedral occupation.

Diffusion experiments [30] have presented data supporting hydrogen occupation of the tetrahedral position of the face-centered-cubic palladium lattice. The diffusion mechanism of hydrogen through palladium occurs via interstitial hopping of the hydrogen from octahedral site to octahedral site via tetrahedral sites, and occupancy therefore becomes an issue of residence time.

In neutron inelastic scattering measurements, the octahedral and tetrahedral optical modes are well separated, which should allow accurate determination of which sites will be preferentially occupied [1].

An excellent overview of other experimental and computational investigations into the question of tetrahedral versus octahedral occupation of palladium by hydrogen isotopes is presented in [2]. The vast majority of studies conclude that tetrahedral site occupancy is impossible, though all conclusions on super-critical data have been based on entirely octahedral or entirely tetrahedral occupation only. Beg *et al.* [31] conclude that mixed octahedral+tetrahedral occupation is the best explanation for their spectroscopic sub-critical measurements of β-PdH_x.

5.2 Structure Factor Rules Governing Octahedral and Tetrahedral Site Occupation of the FCC Lattice

The possibility of tetrahedral occupation then remains somewhat unanswered. This chapter attempts to resolve the question by presenting both fundamental calculations on the effect of octahedral and tetrahedral occupation upon low-order diffraction peak magnitudes, and an evaluation of the diffraction data collected on HIFAR HRPD and ISIS HRPD (see sections 3.6, 3.7, 4.6 and 4.7) specifically in the light of the calculations.

Basic calculations are now presented on the behavior of some diffraction peak magnitudes with octahedral and tetrahedral occupations in FCC palladium-deuterium. Note that the palladium scattering length is approximately equal to the deuterium scattering magnitude.

For the purposes of these calculations, they will be taken as equal. These results will then be compared to the results obtained in the experiments detailed in Chapters 3 and 4

The distance from octahedral site to tetrahedral site is = 2.1Å. The minimum distance from palladium atom to deuterium atom is = 1.7Å

For the $Fm\bar{3}m$ space group, the following rules apply:

The origin is at the center at $m\bar{3}m$.

(0,0,0; 0,½,½; ½,0,½; ½,½,0) ±

$$\begin{vmatrix} x,y,z, & \bar{x},\bar{y},z, & \bar{x},y,\bar{z}, & x,\bar{y},\bar{z}, & y,z,x, & \bar{y},z,\bar{x}, & y,\bar{z},\bar{x}, & \bar{y},\bar{z},x, & z,x,y, & \bar{z},x,\bar{y}, & \bar{z},\bar{x},y, & z,\bar{x},\bar{y}, \\ y,x,z, & \bar{y},\bar{x},z, & \bar{y},x,\bar{z}, & y,\bar{x},\bar{z}, & z,y,x, & \bar{z},y,\bar{x}, & z,\bar{y},\bar{x}, & \bar{z},\bar{y},x, & x,z,y, & \bar{x},z,\bar{y}, & \bar{x},\bar{z},y, & x,\bar{z},\bar{y}, \end{vmatrix} \quad (5.1)$$

The structure factors for the [hkl] peak and an atom at position (x y z) are

$$A = 32\cos^2 2\pi\frac{h+k}{4}\cos^2 2\pi\frac{k+l}{4}\begin{Bmatrix}\cos 2\pi hx\left[\cos 2\pi ky\cos 2\pi lz+\cos 2\pi ly\cos 2\pi kz\right]+\\ \cos 2\pi hy\left[\cos 2\pi kz\cos 2\pi lx+\cos 2\pi lz\cos 2\pi kx\right]+\\ \cos 2\pi hz\left[\cos 2\pi kx\cos 2\pi ly+\cos 2\pi lx\cos 2\pi ky\right]\end{Bmatrix} \quad (5.2)$$

$$B = 0 \quad (5.3)$$

$$F(hkl) = F(\bar{h}\bar{k}l) = F(\bar{h}kl) = F(h\bar{k}l) = F(hk\bar{l}) \quad (5.4)$$

The equivalent positions for the octahedral site are:

(0,0,0)
(½,0,0)
(0,½,0)
(0,0,½)

The equivalent positions for the tetrahedral site are:

(¼,¼,¼)
(¼,¼,¾)
(¼,¾,¼)
(¼,¾,¾)
(¾,¼,¼)
(¾,¼,¾)
(¾,¾,¼)
(¾,¾,¾)

For the 111 peak we have [hkl] = [111]

Then from Eqn (5.2), for any atomic position (x,y,z)

$$A^{111}_{(x\ y\ z)} = \sum_{\text{Equiv (xyz)}} 32\cos^2 2\pi\frac{2}{4}\cos^2 2\pi\frac{2}{4}\begin{Bmatrix}\cos 2\pi x\left[\cos 2\pi y\cos 2\pi z+\cos 2\pi y\cos 2\pi z\right]+\\ \cos 2\pi y\left[\cos 2\pi z\cos 2\pi x+\cos 2\pi z\cos 2\pi x\right]+\\ \cos 2\pi z\left[\cos 2\pi x\cos 2\pi y+\cos 2\pi x\cos 2\pi y\right]\end{Bmatrix}$$

$$= \sum_{\text{Equiv (xyz)}} 32(-1)^2(-1)^2\begin{Bmatrix}\cos 2\pi x\left[\cos 2\pi y\cos 2\pi z+\cos 2\pi y\cos 2\pi z\right]+\\ \cos 2\pi y\left[\cos 2\pi z\cos 2\pi x+\cos 2\pi z\cos 2\pi x\right]+\\ \cos 2\pi z\left[\cos 2\pi x\cos 2\pi y+\cos 2\pi x\cos 2\pi y\right]\end{Bmatrix}$$

$$= \sum_{\text{Equiv (xyz)}} 32\begin{Bmatrix}\cos 2\pi x\left[\cos 2\pi y\cos 2\pi z+\cos 2\pi y\cos 2\pi z\right]+\\ \cos 2\pi y\left[\cos 2\pi z\cos 2\pi x+\cos 2\pi z\cos 2\pi x\right]+\\ \cos 2\pi z\left[\cos 2\pi x\cos 2\pi y+\cos 2\pi x\cos 2\pi y\right]\end{Bmatrix}$$

So, evaluate this expression for each equivalent octahedral position:

Octahedral Position (0,0,0)

$$A^{111}_{(0\ 0\ 0)} = 32\begin{Bmatrix}\cos 2\pi x\left[\cos 2\pi y\cos 2\pi z+\cos 2\pi y\cos 2\pi z\right]+\\ \cos 2\pi y\left[\cos 2\pi z\cos 2\pi x+\cos 2\pi z\cos 2\pi x\right]+\\ \cos 2\pi z\left[\cos 2\pi x\cos 2\pi y+\cos 2\pi x\cos 2\pi y\right]\end{Bmatrix}$$

$$= 32\begin{Bmatrix}\cos 0\left[\cos 0\cos 0+\cos 0\cos 0\right]+\\ \cos 0\left[\cos 0\cos 0+\cos 0\cos 0\right]+\\ \cos 0\left[\cos 0\cos 0+\cos 0\cos 0\right]\end{Bmatrix}$$

$$= 32\{2+2+2\}$$

$$= 192$$

Octahedral Position (½,0,0)

$$A^{100}_{(1/2\ 0\ 0)} = 32\begin{Bmatrix}\cos 2\pi x\left[\cos 2\pi y\cos 2\pi z+\cos 2\pi y\cos 2\pi z\right]+\\ \cos 2\pi y\left[\cos 2\pi z\cos 2\pi x+\cos 2\pi z\cos 2\pi x\right]+\\ \cos 2\pi z\left[\cos 2\pi x\cos 2\pi y+\cos 2\pi x\cos 2\pi y\right]\end{Bmatrix}$$

$$= 32\begin{Bmatrix}\cos \pi\left[\cos 0\cos 0+\cos 0\cos 0\right]+\\ \cos 0\left[\cos 0\cos \pi+\cos 0\cos \pi\right]+\\ \cos 0\left[\cos \pi\cos 0+\cos \pi\cos 0\right]\end{Bmatrix}$$

$$= 32\{-2-2-2\}$$

$$= -192$$

Octahedral Position (0,½,0)

$$A^{111}_{(0\ 1/2\ 0)} = 32\begin{Bmatrix}\cos 2\pi x[\cos 2\pi y \cos 2\pi z + \cos 2\pi y \cos 2\pi z]+\\ \cos 2\pi y[\cos 2\pi z \cos 2\pi x + \cos 2\pi z \cos 2\pi x]+\\ \cos 2\pi z[\cos 2\pi x \cos 2\pi y + \cos 2\pi x \cos 2\pi y]\end{Bmatrix}$$

$$= 32\begin{Bmatrix}\cos 0[\cos \pi \cos 0 + \cos \pi \cos 0]+\\ \cos \pi[\cos 0 \cos 0 + \cos 0 \cos 0]+\\ \cos 0[\cos 0 \cos \pi + \cos 0 \cos \pi]\end{Bmatrix}$$

$$= 32\{-2-2-2\}$$

$$= -192$$

Octahedral Position (0,0,½)

$$A^{111}_{(0\ 0\ 1/2)} = 32\begin{Bmatrix}\cos 2\pi x[\cos 2\pi y \cos 2\pi z + \cos 2\pi y \cos 2\pi z]+\\ \cos 2\pi y[\cos 2\pi z \cos 2\pi x + \cos 2\pi z \cos 2\pi x]+\\ \cos 2\pi z[\cos 2\pi x \cos 2\pi y + \cos 2\pi x \cos 2\pi y]\end{Bmatrix}$$

$$= 32\begin{Bmatrix}\cos 0[\cos 0 \cos \pi + \cos 0 \cos \pi]+\\ \cos 0[\cos \pi \cos 0 + \cos \pi \cos 0]+\\ \cos \pi[\cos 0 \cos 0 + \cos 0 \cos 0]\end{Bmatrix}$$

$$= 32\{-2-2-2\}$$

$$= -192$$

So,

$$A^{111}_{octahedral} = A^{111}_{(0\ 0\ 0)} + A^{111}_{(1/2\ 0\ 0)} + A^{111}_{(0\ 1/2\ 0)} + A^{111}_{(0\ 0\ 1/2)}$$

$$= 192 - 192 - 192 - 192$$

$$= -384$$

Hence, octahedral deuterium will reduce the magnitude of the 111 peak.

For an atom at each equivalent tetrahedral site, the effect on [111] is:

Tetrahedral site (¼,¼,¼)

$$A^{111}_{(1/4\,1/4\,1/4)} = 32\left\{\begin{array}{l}\cos 2\pi x\left[\cos 2\pi y\cos 2\pi z+\cos 2\pi y\cos 2\pi z\right]+\\ \cos 2\pi y\left[\cos 2\pi z\cos 2\pi x+\cos 2\pi z\cos 2\pi x\right]+\\ \cos 2\pi z\left[\cos 2\pi x\cos 2\pi y+\cos 2\pi x\cos 2\pi y\right]\end{array}\right\}$$

$$= 32\left\{\begin{array}{l}\cos\frac{\pi}{2}\left[\cos\frac{\pi}{2}\cos\frac{\pi}{2}+\cos\frac{\pi}{2}\cos\frac{\pi}{2}\right]+\\ \cos\frac{\pi}{2}\left[\cos\frac{\pi}{2}\cos\frac{\pi}{2}+\cos\frac{\pi}{2}\cos\frac{\pi}{2}\right]+\\ \cos\frac{\pi}{2}\left[\cos\frac{\pi}{2}\cos\frac{\pi}{2}+\cos\frac{\pi}{2}\cos\frac{\pi}{2}\right]\end{array}\right\}$$

$$= 32\{0+0+0\}$$

$$= 0$$

Tetrahedral site (¼,¼,¾)

$$A^{111}_{(1/4\,1/4\,3/4)} = 32\left\{\begin{array}{l}\cos 2\pi x\left[\cos 2\pi y\cos 2\pi z+\cos 2\pi y\cos 2\pi z\right]+\\ \cos 2\pi y\left[\cos 2\pi z\cos 2\pi x+\cos 2\pi z\cos 2\pi x\right]+\\ \cos 2\pi z\left[\cos 2\pi x\cos 2\pi y+\cos 2\pi x\cos 2\pi y\right]\end{array}\right\}$$

$$= 32\left\{\begin{array}{l}\cos\frac{\pi}{2}\left[\cos\frac{\pi}{2}\cos\frac{3\pi}{2}+\cos\frac{\pi}{2}\cos\frac{3\pi}{2}\right]+\\ \cos\frac{\pi}{2}\left[\cos\frac{3\pi}{2}\cos\frac{\pi}{2}+\cos\frac{3\pi}{2}\cos\frac{\pi}{2}\right]+\\ \cos\frac{3\pi}{2}\left[\cos\frac{\pi}{2}\cos\frac{\pi}{2}+\cos\frac{\pi}{2}\cos\frac{\pi}{2}\right]\end{array}\right\}$$

$$= 32\{0+0+0\}$$

$$= 0$$

Similarly we find for the tetrahedral positions (¼,¾,¼), (¼,¾,¾), (¾,¼,¼), (¾,¼,¾), (¾,¾,¼), (¾,¾,¾)

$$A^{111}_{(1/4\,3/4\,1/4)} = A^{111}_{(1/4\,3/4\,3/4)} = A^{111}_{(3/4\,1/4\,1/4)} = A^{111}_{(3/4\,1/4\,3/4)} = A^{111}_{(3/4\,3/4\,1/4)} = A^{111}_{(3/4\,3/4\,3/4)}$$

$$= 0$$

and

$$A^{111}_{terahedral} = A^{111}_{(1/4\ 1/4\ 1/4)} + A^{111}_{(1/4\ 1/4\ 3/4)} + A^{111}_{(1/4\ 3/4\ 1/4)} + A^{111}_{(1/4\ 3/4\ 3/4)} +$$
$$A^{111}_{(3/4\ 1/4\ 1/4)} + A^{111}_{(3/4\ 1/4\ 3/4)} + A^{111}_{(3/4\ 3/4\ 1/4)} + A^{111}_{(3/4\ 3/4\ 3/4)}$$
$$= 0 + 0 + 0 + 0 + 0 + 0 + 0 + 0$$
$$= 0$$

Thus, tetrahedral deuterium will have no effect on the (111) peak.

For the [200] peak then [hkl] = [200], and from Eqn (5.2) we have

$$A^{200}_{(x\ y\ z)} = \sum_{\text{Equiv (xyz)}} 32\cos^2 2\pi\frac{2}{4}\cos^2 2\pi\frac{0}{4}\begin{Bmatrix}\cos 4\pi x[\cos 0\cos 0 + \cos 0\cos 0]+\\ \cos 4\pi y[\cos 0\cos 0 + \cos 0\cos 0]+\\ \cos 4\pi z[\cos 0\cos 0 + \cos 0\cos 0]\end{Bmatrix}$$
$$= \sum_{\text{Equiv (xyz)}} 32(-1)^2(1)^2\begin{Bmatrix}\cos 4\pi x[1+1]+\\ \cos 4\pi y[1+1]+\\ \cos 4\pi z[1+1]\end{Bmatrix}$$
$$= \sum_{\text{Equiv (xyz)}} 32\{2\cos 4\pi x + 2\cos 4\pi y + 2\cos 4\pi z\}$$

Firstly, calculate this for the equivalent octahedral sites.

For octahedral position (0,0,0)

$$A^{200}_{(0\ 0\ 0)} = 32\{2\cos 4\pi x + 2\cos 4\pi y + 2\cos 4\pi z\}$$
$$= 32\{2\cos 0 + 2\cos 0 + 2\cos 0\}$$
$$= 32\{2 + 2 + 2\}$$
$$= 192$$

Octahedral position (½,0,0)

$$A^{200}_{(1/2\ 0\ 0)} = 32\{2\cos 4\pi x + 2\cos 4\pi y + 2\cos 4\pi z\}$$
$$= 32\{2\cos 2\pi + 2\cos 0 + 2\cos 0\}$$
$$= 32\{2 + 2 + 2\}$$
$$= 192$$

Similarly, for octahedral position (0,½,0) and (0,0,½)

$$A^{200}_{(0\ 1/2\ 0)} = A^{200}_{(0\ 0\ 1/2)} = 192$$

$$A^{200}_{octahedral} = A^{200}_{(0\ 0\ 0)} + A^{200}_{(1/2\ 0\ 0)} + A^{200}_{(0\ 1/2\ 0)} + A^{200}_{(0\ 0\ 1/2)}$$
$$= 192 + 192 + 192 + 192$$
$$= 768$$

Thus, octahedral deuterium will add magnitude to the 200 peak.

Now consider the tetrahedral positions effect on [200].

For tetrahedral site (¼,¼,¼)

$$A^{200}_{(¼\ ¼\ ¼)} = 32\{2\cos 4\pi x + 2\cos 4\pi y + 2\cos 4\pi z\}$$
$$= 32\{2\cos\pi + 2\cos\pi + 2\cos\pi\}$$
$$= 32\{-2-2-2\}$$
$$= -192$$

For tetrahedral site (¼,¼,¾)

$$A^{200}_{(¼\ ¼\ ¾)} = 32\{2\cos 4\pi x + 2\cos 4\pi y + 2\cos 4\pi z\}$$
$$= 32\{2\cos\pi + 2\cos\pi + 2\cos 3\pi\}$$
$$= 32\{-2-2-2\}$$
$$= -192$$

Similarly for tetrahedral positions (¼,¾,¼), (¼,¾,¾), (¾,¼,¼), (¾,¼,¾), (¾,¾,¼), (¾,¾,¾)

$$A^{200}_{(¼\ ¼\ ¾)} = A^{200}_{(¼\ ¾\ ¾)} = A^{200}_{(¾\ ¼\ ¼)} = A^{200}_{(¾\ ¼\ ¾)} = A^{200}_{(¾\ ¾\ ¼)} = A^{200}_{(¾\ ¾\ ¾)} =$$
$$= -192$$

and

$$A^{200}_{tetrahedral} = \sum_{\text{Equiv (xyz)}} A^{200}_{(x\ y\ z)}$$
$$= -192 - 192 - 192 - 192 - 192 - 192 - 192 - 192$$
$$= -1536$$

Thus tetrahedral deuterium will decrease the magnitude of the [200] peak

For the [220] peak then [hkl] = [220], and from Eqn (5.2) we have

$$A^{220}_{(x\ y\ z)} = \sum_{\text{Equiv (xyz)}} 32\cos^2 2\pi\frac{4}{4}\cos^2 2\pi\frac{2}{4}\begin{Bmatrix}\cos 4\pi x\left[\cos 4\pi y\cos 0+\cos 0\cos 4\pi z\right]+\\ \cos 4\pi y\left[\cos 4\pi z\cos 0+\cos 0\cos 4\pi x\right]+\\ \cos 4\pi z\left[\cos 4\pi x\cos 0+\cos 0\cos 4\pi y\right]\end{Bmatrix}$$

$$= \sum_{\text{Equiv (xyz)}} 32(1)^2(-1)^2\begin{Bmatrix}\cos 4\pi x\left[\cos 4\pi y+\cos 4\pi z\right]+\\ \cos 4\pi y\left[\cos 4\pi z+\cos 4\pi x\right]+\\ \cos 4\pi z\left[\cos 4\pi x+\cos 4\pi y\right]\end{Bmatrix}$$

$$= \sum_{\text{Equiv (xyz)}} 32\begin{Bmatrix}\cos 4\pi x\left[\cos 4\pi y+\cos 4\pi z\right]+\\ \cos 4\pi y\left[\cos 4\pi z+\cos 4\pi x\right]+\\ \cos 4\pi z\left[\cos 4\pi x+\cos 4\pi y\right]\end{Bmatrix}$$

Determine the value of A^{220} for the octahedral sites.

For octahedral position (0,0,0)

$$A^{220}_{(0\ 0\ 0)} = 32\begin{Bmatrix}\cos 4\pi x\left[\cos 4\pi y+\cos 4\pi z\right]+\\ \cos 4\pi y\left[\cos 4\pi z+\cos 4\pi x\right]+\\ \cos 4\pi z\left[\cos 4\pi x+\cos 4\pi y\right]\end{Bmatrix}$$

$$= 32\{\cos 0[\cos 0+\cos 0]+\cos 0[\cos 0+\cos 0]+\cos 0[\cos 0+\cos 0]\}$$

$$= 32\{2+2+2\}$$

$$= 192$$

For octahedral position (½,0,0)

$$A^{220}_{(\frac{1}{2}\ 0\ 0)} = 32\begin{Bmatrix}\cos 2\pi\left[\cos 0+\cos 0\right]+\\ \cos 0\left[\cos 0+\cos 2\pi\right]+\\ \cos 0\left[\cos 2\pi+\cos 0\right]\end{Bmatrix}$$

$$= 32\{2+2+2\}$$

$$= 192$$

Similarly, for octahedral positions (0,½,0),(0,0,½)

$$A^{220}_{(0\ \frac{1}{2}\ 0)} = A^{220}_{(0\ 0\ \frac{1}{2})} = 192$$

$$A^{220}_{octahedra} = \sum_{\text{Equiv (xyz)}} A^{220}_{(x\ y\ z)}$$

$$= 192+192+192+192$$

$$= 768$$

Thus octahedral occupation adds magnitude to the [220] peak

Now for the effect of tetrahedral sites on [200]

For tetrahedral site (¼,¼,¼)

$$A^{220}_{(¼,¼,¼)} = 32\begin{Bmatrix}\cos\pi[\cos\pi+\cos\pi]+\\ \cos\pi[\cos\pi+\cos\pi]+\\ \cos\pi[\cos\pi+\cos\pi]\end{Bmatrix}$$
$$= 32\{-1[-1-1]-1[-1-1]-1[-1-1]\}$$
$$= 32\{2+2+2\}$$
$$= 192$$

For tetrahedral site (¼,¼,¾)

$$A^{220}_{(¼,¼,¾)} = 32\begin{Bmatrix}\cos\pi[\cos\pi+\cos 3\pi]+\\ \cos\pi[\cos 3\pi+\cos\pi]+\\ \cos 3\pi[\cos\pi+\cos\pi]\end{Bmatrix}$$
$$= 32\{-1[-1-1]-1[-1-1]-1[-1-1]\}$$
$$= 32\{2+2+2\}$$
$$= 192$$

Similarly for tetrahedral positions (¼,¾,¼), (¼,¾,¾), (¾,¼,¼), (¾,¼,¾), (¾,¾,¼), (¾,¾,¾)

$$A^{220}_{(¼,¾,¼)} = A^{220}_{(¼,¾,¾)} = A^{220}_{(¾,¼,¼)} = A^{220}_{(¾,¼,¾)} = A^{220}_{(¾,¾,¼)} = A^{220}_{(¾,¾,¾)} = 192$$

and

$$A^{220}_{tetrahedral} = \sum_{\text{Equiv (xyz)}} A^{220}_{(x\ y\ z)}$$
$$= 192+192+192+192+192+192+192+192$$
$$= 1536$$

Thus tetrahedral deuterium will add magnitude to the [220] peak

The results for all peaks and both sites are summarised in Table 6.1

Table 5.1: Effects of special position occupations on major peak heights

	octahedral	tetrahedral
[111]	Decrease (-384)	No effect (0)
[200]	Increase (+768)	Decrease (-1536)
[220]	Increase (+768)	Increase (+1536)

In our case, actual deuterium concentration is known from the manometry of the Sieverts apparatus. Accurate Rietveld refinement of the [111] peak profile and height reveals the amount of this deuterium located in octahedral sites of the palladium FCC lattice, and any excess must be located in tetrahedral sites. This is essentially the method used to refine the collected patterns for the purpose of investigating tetrahedral occupation.

We can estimate the probable influence of tetrahedral occupation on the measured peak height ratios. With tetrahedral occupation in evidence, the measured height of the [111] peak will be higher than expected (as there will be less octahedral deuterium than expected), the height of [200] will be lower than expected and the height of [220] will be higher than expected. So the ratio of [111] peak height over [200] peak height ([111]/[200]) would appear larger than expected. Similarly [200]/[220] will be lower than expected. Since both the [111] peak height, and the [220] peak height will be larger than with entirely octahedral occupation, it is difficult to judge the outcome in the case of [111]/[220].

These results are used in the following section of this chapter where experimentally measured peak heights are compared to calculated heights.

5.3 A Comparison of Calculated Peak Heights and Experimentally Measured Peak Heights.

Using the Rietica program, neutron diffraction patterns were calculated for PdH_x ($1 \geq x \geq 0$; in steps of 0.05), using reasonable thermal parameters and the approximate lattice parameter (determined from ADF/BAND calculations – see Chapter 6), for both time-of-flight (ToF) and constant-wavelength diffractometers. For each concentration the ratio of the peak heights of the lattice reflections 111, 200 and 220 were calculated and plotted against concentration (i.e. max(111)/max(200), max(111)/max(220),

max(200)/max(220)). These were then compared to the measured peak heights from the experiments performed on HIFAR HRPD and ISIS HRPD

The calculated peak profiles for the time-of-flight instrument ISIS HRPD are shown in Fig 5.2. All of the [111], [200] and [220] peaks are plotted in Fig 5.2 for all deuterium to metal concentrations considered, and considering octahedral occupation only. The instrumental peak-profile parameters from ISIS HRPD were used, along with reasonable thermal parameters to give an approximation of what the collected diffraction peaks should look like. Note that as the lattice parameter increases with increasing D/Pd concentration, the peaks are all shifted towards the right with increasing concentration. So we can determine from this figure that increasing deuterium concentration in an octahedral only model reduces the height of the [111] peak, and increases the height of both [200] and [220]. Fig 5.3 plots the expected *relative* peak heights for these three peaks.

The calculations were also performed for the constant-wavelength instrument HIFAR HRPD. The relative peak heights for the constant-wavelength instrument are shown in Fig 5.4

We can now measure the peak heights from collected patterns, calculate the relative peak heights from these and compare them to those expected. This will allow us to make some comparisons and conclusions about the collected patterns compared to the octahedral only model

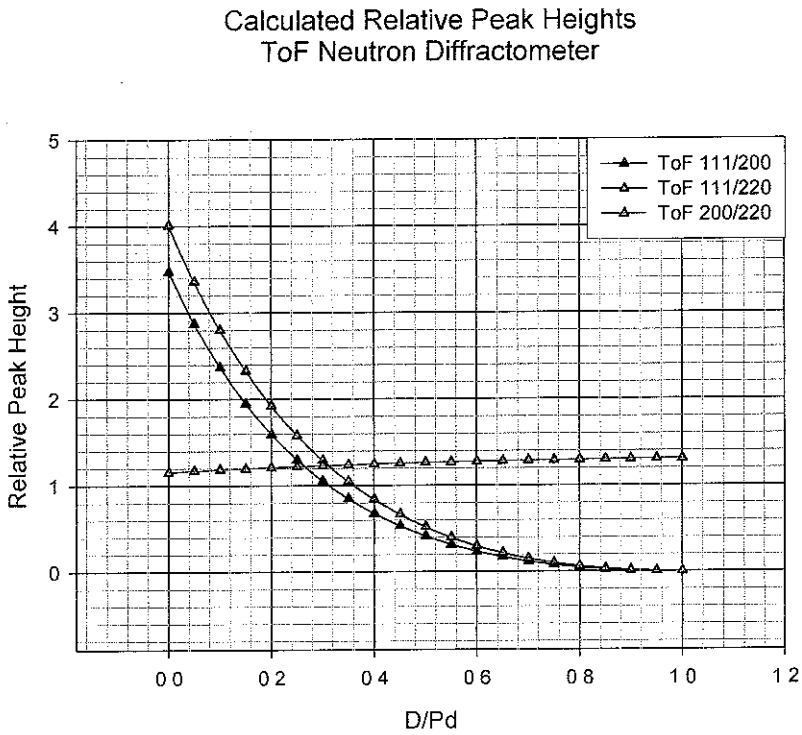

Fig 5 3 Palladium-deuterium: Relative peak heights of the three lowest order peaks for a time-of-flight neutron beam diffractometer using an octahedral model only The instrument dependent parameters were taken from the ISIS HRPD instrument

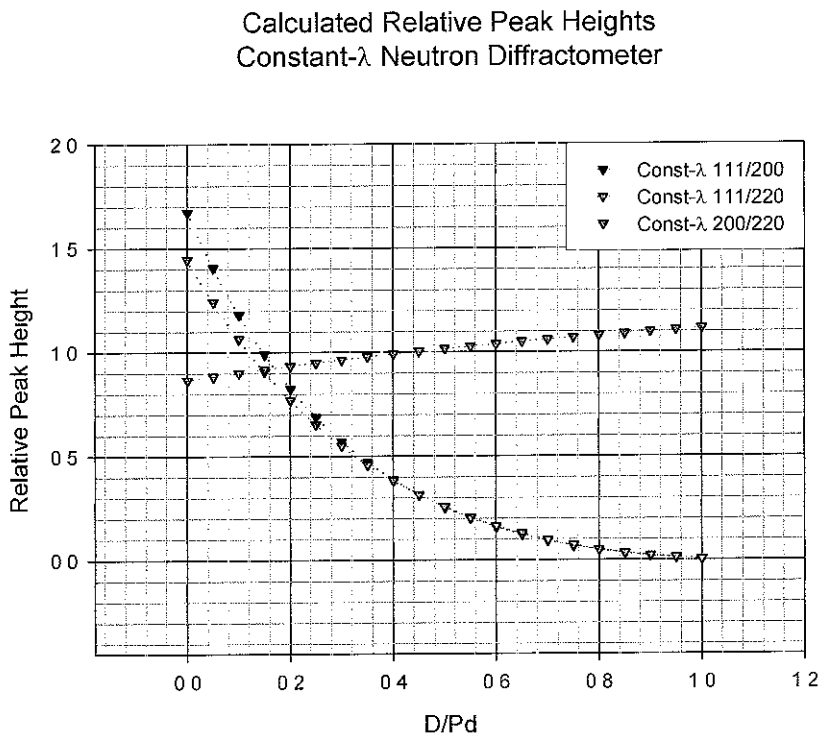

Fig 5.4 Palladium-deuterium: Relative peak heights of the three lowest order peaks for a constant wavelength neutron beam diffractometer using an octahedral model only. The instrument dependent parameters were taken from the HIFAR HRPD instrument.

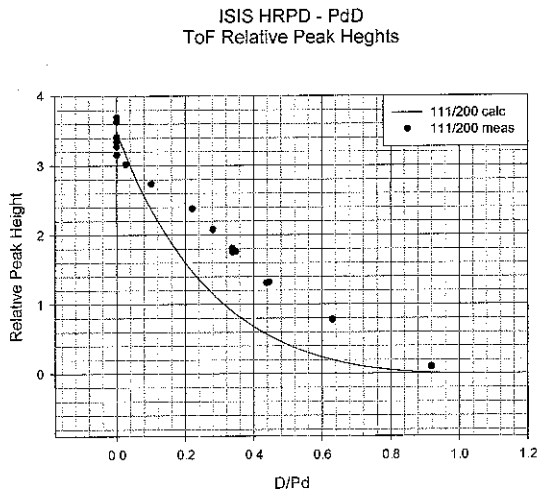

a)

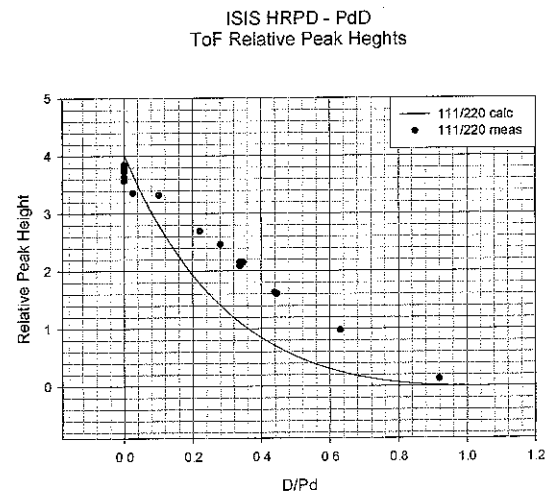

b)

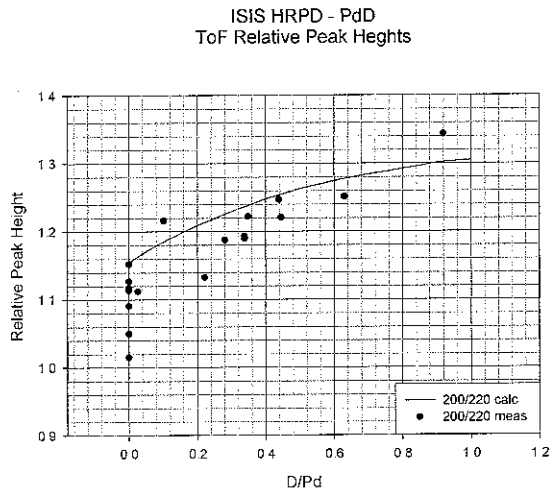

c)

Fig 5 5 Relative peak height comparisons for a time-of-flight neutron diffractometer, expected and experimental Solid line is expected behaviour for an octahedral only model Points are experimental results from ISIS HRPD a) peak height 111/200 b) peak height 111/220 c) peak height 200/220

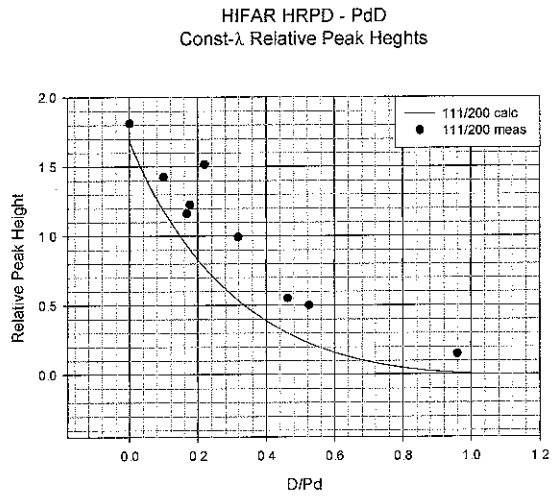

a)

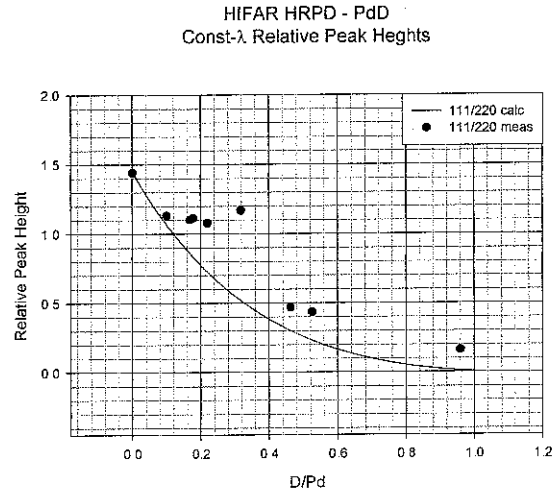

b)

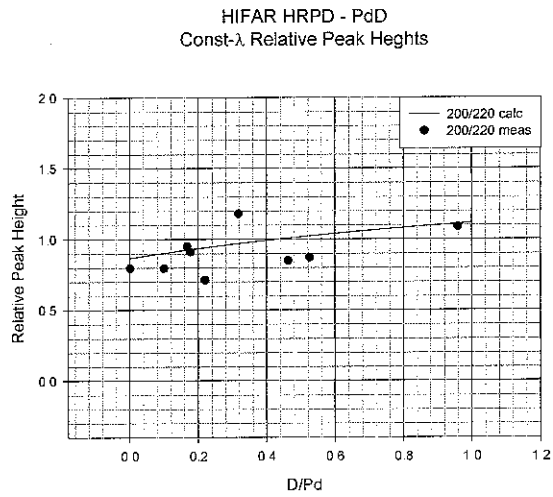

c)

Fig 5 6 Relative peak height comparisons for a constant-wavelength neutron diffractometer, expected and experimental Solid line is expected behaviour for an octahedral only model Points are experimental results from HIFAR HRPD a) peak height 111/200 b) peak height 111/220 c) peak height 200/220

There are only two sites in the face-centered-cubic structure available for the deuterium atom to occupy, those being the octahedral site and the tetrahedral position. In both Fig 5 5 a) and 5 6 a) above, the measured ratio of [111] peak height over [200] peak height all lie above the calculated line. This indicates that the intensity of the [111] peak is higher than expected. Based on the results of Table 6.1, since octahedral occupation reduces the [111] peak height and tetrahedral occupation does not affect [111] height, then the occupation of octahedral positions is lower than expected. This is an indicator of tetrahedral occupation

In Figs 5.5 c) and 5.6 c), the ratio of [200] peak height over [220] peak height is generally less than that for the octahedral-only model. As shown at the end of section 5.2, based on similar arguments to those in the preceding paragraph here, this is also an indicator of tetrahedral occupation in these two experiments.

The measured [111]/[220] peak heights as seen in Figs 5.5 b) and 5.6 b) tend to lie above the calculated line, showing that the [111] peak height is relatively higher than expected in comparison to the [220] peak height. No positive conclusion can be made from this in regards to tetrahedral occupation, though it is possible that a similar effect to that governing the [111]/[200] relative peak height is in operation.

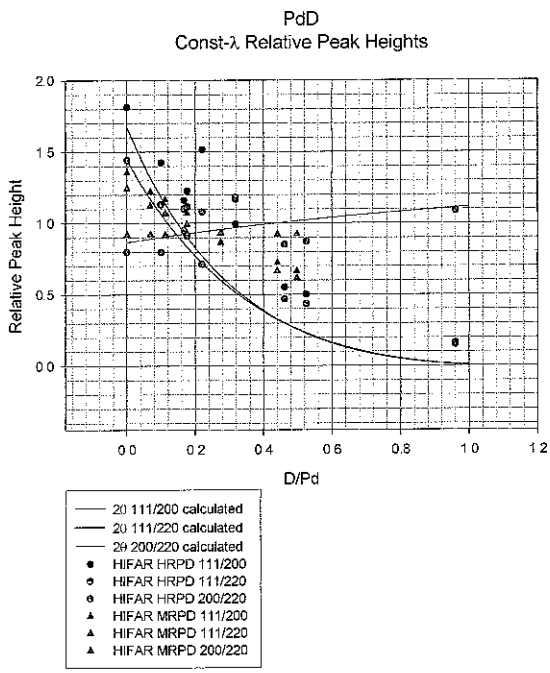

Fig 5.7 Relative peak height comparisons for a constant-wavelength neutron diffractometer, expected and experimental. Solid line is expected behaviour for an octahedral only model. Points are experimental results from HIFAR HRPD (circles) and HIFAR MRPD (triangles).

The actual D/Pd is known from manometric measurements (described in Chapter 3), and any excess must be in tetrahedral sites, so it should be possible to accurately refine both the octahedral site occupation numbers and the tetrahedral site occupation numbers.

Fig 5.7 shows all of the results of Fig 5.6, along with some of the experimental results obtained from the HIFAR MRPD instrument in [2]. It can be seen that these also follow the same trend as described in the preceding paragraphs for the two HRPD instruments (HIFAR and ISIS), though the results are less reliable for MRPD as the calculated patterns are based on the HIFAR HRPD instrument.

5.4 Procedure for Analysing High Resolution Data

From section 5.2 above, summarized in Table 5.1, octahedral site occupation affects peak [111] (decreasing it), peak [200] (reinforcing it) and peak [222] (reinforce). Tetrahedral site occupation does not affect [111], but alters [200] (decrease) and [222] (increase). We can use these facts to determine the amount of tetrahedral site occupation at each deuterium-to-palladium concentration. Firstly, the exact deuterium concentration is known from manometric measurements as described in Chapter 3. Collected patterns are refined until a good fit is obtained on the [111] peak using an octahedral only model. Any discrepancy between the manometric deuterium concentration, and the refined deuterium concentration must then be accounted for by tetrahedral site occupation.

The procedure for refining the patterns with the aim of determining tetrahedral occupancies is as follows. Model the palladium phase with the usual *FM3M* space group. Refine only one (or two) of the parameters at any time. Use a LeBail fit for the stainless steel phase resulting from the sample container. Constrain the octahedral site thermal parameter to be 3.4 times the tetrahedral site thermal parameter i.e. the square of the ratio of the octahedral and tetrahedral interstitial hole sizes.

First, refine the lattice parameter of the palladium phase until a reasonable fit is obtained. The structure factor rules calculated above show that the [111] palladium peak will be affected by octahedral deuterium occupation only and unaffected by tetrahedral deuterium occupation. Therefore, refine deuterium occupation of the octahedral site until a good fit is achieved to the intensity of [111]. Calculate the deuterium to palladium concentration from octahedral occupation, compare to the manometric calculations, and assign any missing D/Pd to the tetrahedral site. Then refine (separately) lattice parameter, phase scale, background, thermal parameters, preferred orientation and sample dependent peak-shape parameters. Then return to refine the octahedral occupation, paying attention primarily to the height of the [111] peak and reiterate the process until an excellent fit to the overall pattern is achieved, ensuring that any one refined parameter improves the goodness-of-fit parameters.

Two-phase palladium-deuterium patterns are problematic in that an amount of tetrahedral occupation (versus octahedral) is present in each phase. We have assumed that tetrahedral occupation will only occur in the super-critical region of the phase-diagram, and for this reason octahedral-only occupation was used in refining the patterns collected at 120°C,

with lattice parameter determination the main focus of the refinements (see Section 4.7.3). Although difficult, the technique was used successfully on the two-phase patterns collected at 310°C.

5.5 Refined Occupancies

We have shown in Chapter 4 that in the case of palladium-hydrogen there is a region above the critical temperature, as obtained from p-c-T data, where there exists two very similar, yet distinct, phases. Tetrahedral occupation occurs to reduce the overall energy (strain vs band structure) with maximum tetrahedral site occupation at D/Pd ≈ 0.5 reducing the total deuterium-deuterium interactions. As the palladium-deuterium system approaches D/Pd=1 (NaCl structure) the minimum configuration is all deuterium occupying octahedral positions.

Feenstra et al [32] measured a lattice expansion anomaly at 590 K (critical temp given as 567.5 ± 0.5 K) which they explain as spatial inhomogeneities, but is also a manifestation of two-phase systems.

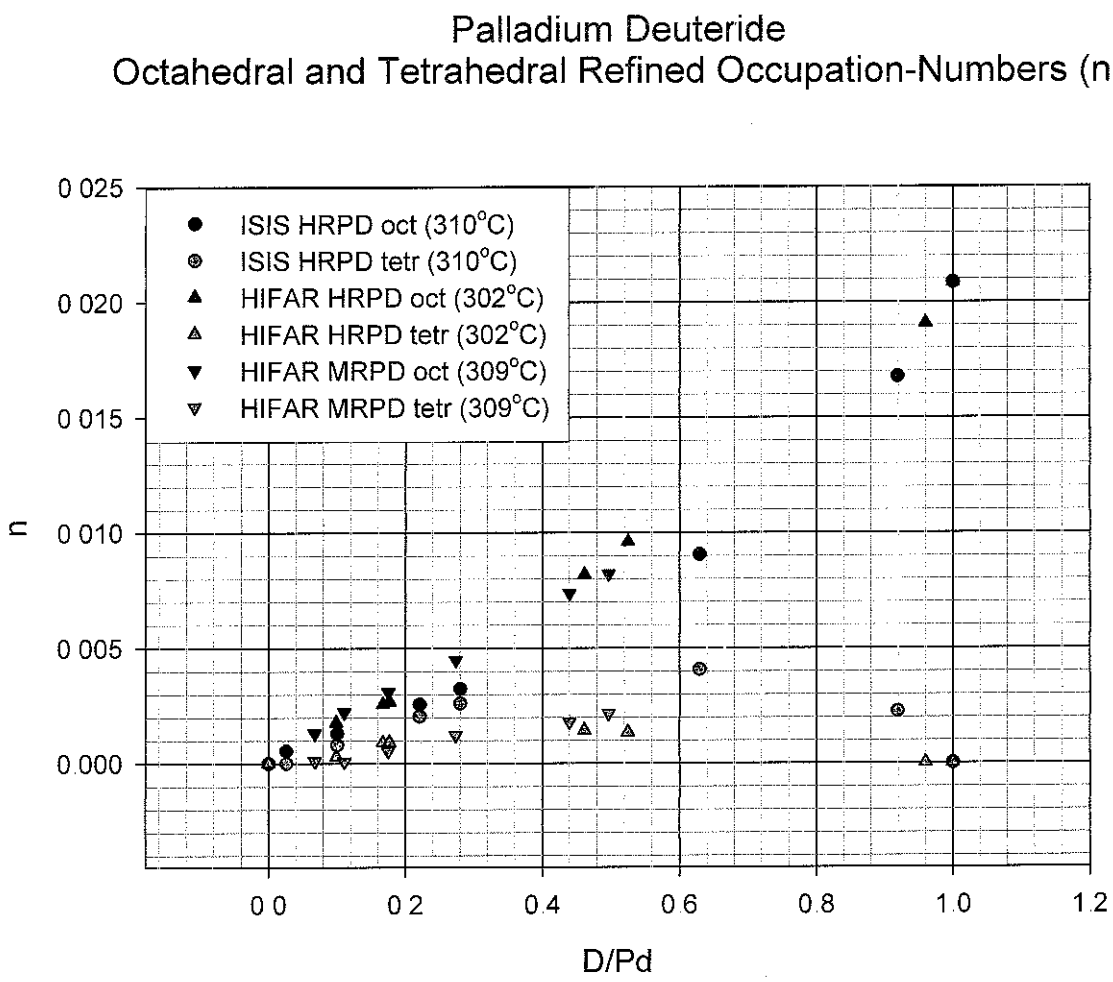

Fig 5 8: Palladium-deuterium system. Deuterium octahedral site and tetrahedral site occupation numbers near the system critical temperature. ISIS HRPD and ANSTO HRPD results are from this thesis (see sections 3 7 and 3 6 respectively). ANSTO MRPD results are from [2]

The results of refining the octahedral and tetrahedral site occupation numbers is shown in Fig 5.8. The results obtained from ISIS HRPD in March/April 2004 and HIFAR HRPD in October 2003 are shown. The refinement strategy was also applied to the results obtained on HIFAR MRPD in [2], and these results have been included. We see an increase in both octahedral and tetrahedral occupation with increasing deuterium concentration in all cases up to $D/Pd \approx 0.5$. The higher the temperature, the more commensurate the tetrahedral occupation number is in comparison to the octahedral site occupation number.

Fig 5 8 suggests that increasing temperature is responsible for an increase in the tetrahedral site occupation, although the effects of the widely different instrument resolutions may also be a factor. This will be in part due to higher thermal energy increasing the rate of diffusion of deuterium from octahedral-site to neighbouring octahedral-site via tetrahedral sites

The results from PSI HRPT at 320°C show that the effect has disappeared by this temperature in this different sample, as the manometric deuterium-to-palladium concentrations were consistently lower than those that could be refined from octahedral or tetrahedral site occupation models. This could however be a result of unknown impurities in the sample, as was hinted at in Chapter 4, otherwise it suggests that is there a relationship between critical temperature and tetrahedral occupancy.

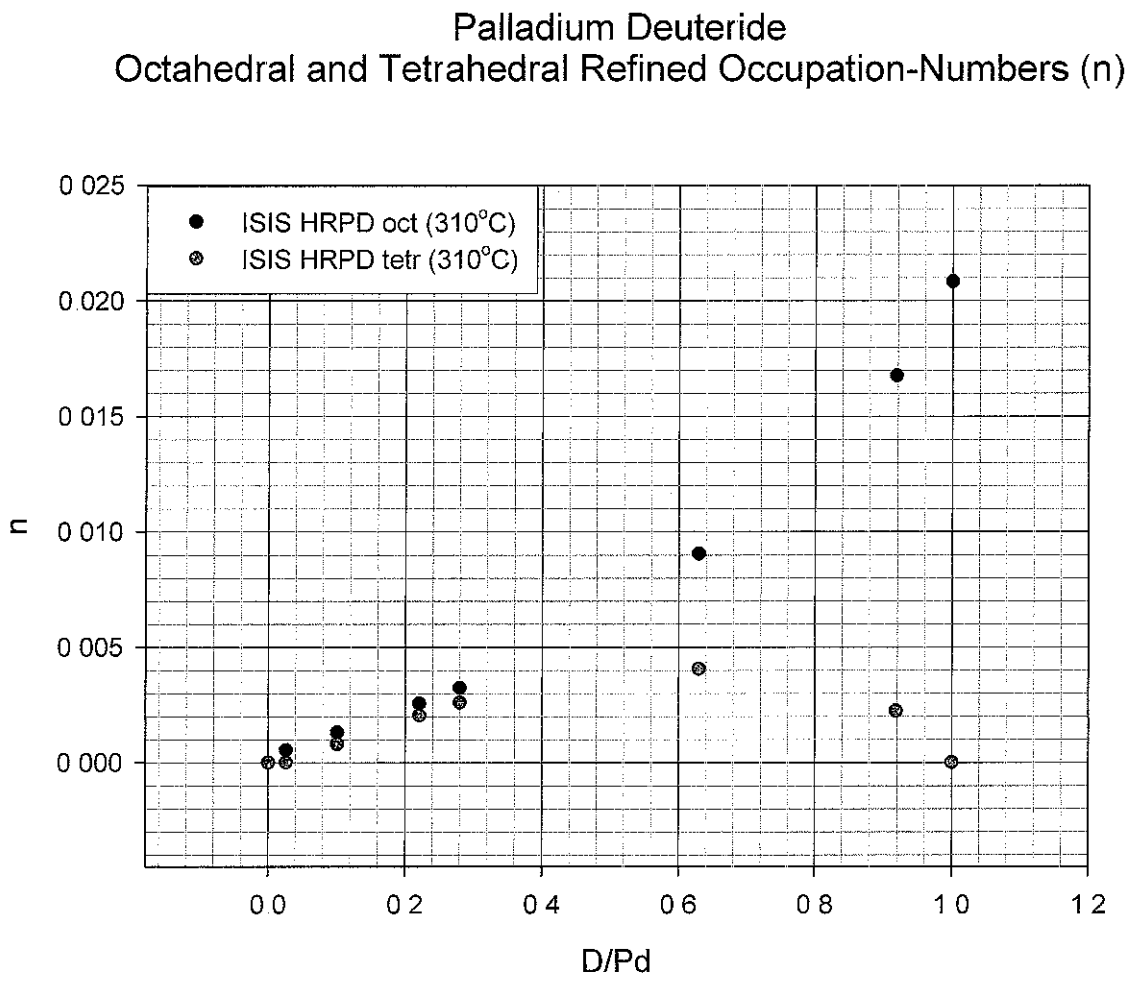

Fig 5 9: Palladium-deuterium System: Single-phase deuterium octahedral site and tetrahedral site occupation numbers at 310°C

Fig 5.9 shows the octahedral-site occupation number and the tetrahedral-site occupation number refined from the single-phase patterns collected on ISIS HRPD in April/May 2004. It has been assumed that at D/Pd=1.0, all of the deuterium present will be occupying the octahedral sites. These are the actual occupation numbers, not the symmetry-reduced occupations as used by Rietica, and so are directly analogous to the relative deuterium concentration present at each site.

At temperatures well below the critical temperature, the stress induced by the different lattice parameters of the α-phase and β-phase is relieved by the formation of dislocations. In the peri-critical region, the difference between the two phases is minimal, and the relatively small stresses are not enough to cause dislocations.

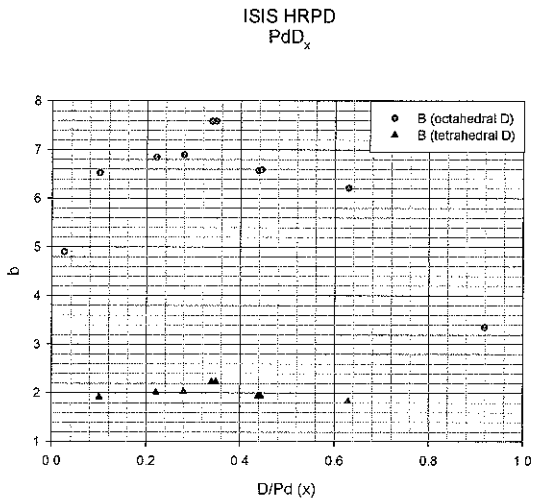

Fig 5.10: Thermal parameters of octahedral and tetrahedral located deuterium in palladium at 310°C

Fig 5.10 shows the thermal parameters refined from the ISIS HRPD data. The thermal parameters from the octahedral site and the tetrahedral site stay constant, apart from the end points, where tetrahedral occupation was not found and the octahedral thermal parameter is at a minimum, and the small bump around D/Pd~0.34 indicating the two-phase region.

5.6 Conclusions and Discussion

This chapter has presented evidence for the occupation by deuterium of the palladium FCC tetrahedral sites during hydrogenation. The experimental evidence, gained from full Rietveld refinement of the diffraction patterns, is consistent with the fundamental calculations performed on the effect of tetrahedral site occupation on the three lowest order peaks of the FCC lattice ([111], [200] and [220]). The occupation of the tetrahedral sites by deuterium seems to be a feature of the peri-critical region of palladium-deuterium (see Chapter 4 for more details on the peri-critical region).

We have presented a useful technique for determining deuterium occupation of both the octahedral and tetrahedral sites of the palladium FCC lattice. This technique has been used to investigate the octahedral site occupation versus tetrahedral site occupation in three palladium samples on a number of the highest resolution neutron-beam diffactometers available. Tetrahedral occupation has been evidenced in two of the three samples, all comprising finely divided palladium. Tetrahedral site occupation was not observed in the experiment on the SINQ HRPT instrument but this could be sample related or owing to the higher sample temperature.

Tetrahedral occupation is understandable as a by-product of local diffusion. Up to a deuterium concentration of 0.5, for each octahedral site occupied, the majority of the nearest neighbor octahedral sites are empty. At high temperatures near the critical temperature, the octahedral deuterium will easily hop between octahedral sites via tetrahedral sites. If the tetrahedral site residency time is long enough compared to octahedral site residency time, the tetrahedral occupation will appear in the diffraction patterns. The maximum tetrahedral occupancy is reached at a deuterium to palladium concentration of 0.5, when we expect the flux of diffusing atoms to be a maximum (number of occupied sites equals number of empty sites.

As the deuterium concentration exceeds 0.5, the majority of nearest neighbour octahedral sites are occupied. This will limit the amount of local hopping and thus limit the opportunity for tetrahedral site occupation.

Chapter 6 introduces some computational studies that find a self-trapping effect on deuterium in the FCC palladium tetrahedral site. This lowers the tetrahedral site energy until it is comparable to the octahedral site energy. In this situation, it is conceivable that deuterium would randomly occupy octahedral and tetrahedral sites, with the two total

amounts of occupation (i.e. in *moles* of deuterium) roughly equal as in the results of April/May 2004 at ISIS. This would continue until local diffusion of deuterium is hindered by a decreasing availability of empty nearest-neighbour octahedral sites as the deuterium concentration increases above 0.5. The repulsive deuterium-deuterium interaction will ensure that with increasing concentration, the deuterium atoms will prefer to occupy the octahedral sites as the NaCl structure is approached at stoichiometric PdD.

Further work in this area should include a high-resolution neutron-beam diffraction study of palladium-deuterium in the temperature range 300°C - 330°C to determine the lattice-parameter derived critical temperature, and to determine if tetrahedral site occupation is a feature of the peri-critical region only, or if it continues into the super-critical region

1 Anderson, I , in *Neuron Scattering from Hydrogen in Metals (Proceedings of the Second Zuoz Summer School on Neutron Scattering)*, A Furrer, Editor. 1994, World Scientific: Singapore. p 142-167

2 Pitt, M P. and E.M.A. Gray, Europhysics Letters, 2003. **64**(3): p 344-350.

3 Pitt, M.P., Thesis 2003, Griffith University: Brisbane.

4 McKeehan, L W , Physical Review, 1923. **21**: p. 334

5 Maeland, A.J. and T R.P j. Gibbs, Journal of Physical Chemistry, 1961. **61**: p. 1270.

6 Worsham, J.E , M.K. Wlkinson, and C G. Shull, J Phys Chem. Solids, 1957 **3**: p. 303-310.

7 Bergsma, J. and J.A. Goedkoop, Physica, 1960 **26**: p. 744-750.

8 Mukhopadhyay, R., et al., Solid State Communications, 1990. **75**: p 359

9 Bennington, S.M , et al., Journal of Electro Chemistry, 1990. **281**: p 323.

10 Nace, D.M. and J.G Ason, Journal of the American Chemical Society, 1957 **79**: p. 3623

11 Ferguson, G.A., et al., Pysical Review A, 1965 **137**: p. 483.

12 Entin, I R., et al., Sov Phys. Solid State, 1974. **15**: p. 1840.

13 Mueller, M H., et al., Acta Cryst A, 1975 **31**: p. S99

14 Anderson, I S., D K. Ross, and C.J. Carlile, Phys. Lett , 1978. **68A**(2): p. 249.

15 Anderson, I.S., C.J. Carlile, and D K. Ross, J. Phys. C: Solid State Phys., 1978. **11**: p. L381.

16 Blaschko, O , et al., Solid State Communications, 1978. **27**: p. 1149

17 Mueller, M H., et al , AIP Conf. Proc , 1979. **53**: p 391.

18 Ellis, T.E , et al., Phys Rev Lett., 1979. **42**(2): p 456

19 Blaschko, O., et al., J. Phys. FL Metal Phys , 1979. **9**(6): p L113

20 Blaschko, O , et al , Acta Cryst. A, 1980. **36**: p. 605.

21 Blaschko, O., P Fratzl, and R. Klemencic, Phys. Rev B, 1981 **24**: p 277

22 Ross, D K., et al., J. Alloys Comp , 1991 **172-174**: p. 169.

23 Lawson, A.C., et al , J Alloys Comp , 1992. **183**: p. 174

24 Wu, E , et al., J. Alloys Comp , 1995. **231**: p. 108

25 Kennedy, S.J , et al., J. Phys : Condens Matter, 1995. **7**: p. L33

26 Wu, E., et al , J. Phys : Condens. Matter, 1996. **8**: p. 2807.

27 King, H W. and F D. Manchester, Journal of Physics F, 1978. **8**: p 15.

28 Jacobs, J.K. and F.D Manchester, J Less-Common Met , 1976 **49**: p. 67.

29 Nelin, G., Phys. Stat. Sol., 1971 **45**: p. 527.

30 Davis, W.D , *Knolls Atomic Power Laboratory Report No. 1227*. 1954

31 Beg, M M. and D K. Ross, J Phys C: Solid State Phys , 1970 **3**: p. 2487.

32 Feenstra, R , D G.d. Groot, and R Griessen, Journal of the Less-Common Metals, 1984. **104**: p 43-49

Chapter Six

A Computational Study of the Peri-Critical Region of the Palladium-Hydride System Using Density Functional Theory Techniques

Chapter Six

A Computational Study of the Peri-Critical Region of the Palladium-Hydride System Using Density Functional Theory Techniques

6.1 Introduction

There are a number of published computational studies into palladium-hydrogen which consider the position of the hydrogen atoms in the palladium lattice [1-6]. Knowing that diffusion between octahedral sites occurs through tetrahedral sites, the expectation was that the tetrahedral site should display favourable energetics and long residence times. To show a significant self-trapping effect where tetrahedral site occupation leads to a local relaxation around the site and a lowering of the sites energy [2, 6]. The tetrahedral site energy can be lowered to be essentially equal to the octahedral site energy. Bound states are found for deuterium, but not hydrogen in [2], and for all hydrogen isotopes but not muons or pions in [6].

There is thus a theoretical basis for tetrahedral occupancy, although it is not clear how realistic it is. Density Functional Theory (DFT) was used as the computational basis for the theoretical study of palladium-hydrogen over other schemes, as it provides a computationally less intensive method for performing the large number of calculations required. Many of the single point calculations presented in this chapter were performed on a standard desktop personal computer, though they could take several days to complete. First-principles calculations on the number of data points required here could not possibly have been done on the computer resources available to the author.

Although DFT is a zero temperature technique it can be used to model the single-phase region above the thermodynamic critical temperature with several stoichiometries Pd_nH_m. The mixed-phase regions are intractable without the availability of much larger unit-cells requiring much greater computing power.

6.1.1. Density Functional Theory

DFT is a computational method for overcoming the many-body problem, which arises when considering the numerous systems reliant upon the behaviour of electrons interacting via Coulombs Law:

$$\hat{V}_{ee} = \frac{1}{2}\sum_{i}\sum_{i\neq j}\frac{1}{|r_i - r_j|} \tag{6.1}$$

For systems neither small nor homogenous, insurmountable problems arise if the methodology is to construct and operate on many-body wavefunctions. For a many-body system (> 2 particles) it is in fact impossible to solve the Hamiltonian exactly. In Electron DFT [7], the many bodied electronic wavefunction is approximated by the single-body electron density functional

6.1.2 The Hartree Approximations

The simplest method of calculating a many-body wavefunction is to assume that it is comprised of the *products* of single-body wavefunctions. However, this models *non-interacting* particles and is therefore not suitable for electronic systems. The 'Naive Hartree' scheme is to approximate a systems total energy, E^{NH}, via the following equation

$$E^{NH} = T_S + V + E_H|n(r)| \tag{6.2}$$

where T_s is the kinetic energy part of the system, V is the external potential and E_H is an additional term caused by the potential set up by the charge density of all the occupied orbitals. This wavefunction does not contain the required antisymmetry under exchange of particle labels as required for fermions.

The Hartree-Fock approach is to construct the many-body wavefunction as the *Slater-determinant* of a matrix of single-body wavefunctions. This does have the required antisymmetry under exchange of wavefunctions, as the determinant of a matrix changes sign whenever a pair of rows or columns is swapped.

6.1.3 Exchange and Correlation

The Pauli principle excludes two electrons of the same spin from being in the same place at the same time. This tendency for two electrons of the same spin to avoid each other is termed *exchange* and decreases the energy of the two electrons by reducing the positive coulomb repulsion between them. This decrease in energy is the *exchange energy*. It is purely quantum mechanical effect and cannot be explained classically.

Electrons of opposite spin are discouraged from occupying the same space not by Pauli, but by electrostatic repulsion. This is termed *correlation* and also decreases the energy of a pair of electrons. The decrease is termed the *correlation energy*. Part of correlation is a classical repulsion effect, and part is a quantum effect caused by the increase in kinetic energy of fermions excluded from each others vicinity. In general, any force between two particles causes classical correlation.

The deficit of other electrons around a localized electron due to exchange is called the *exchange* hole. The similar reduction caused by correlation effects is called the *correlation* hole. Increasing the kinetic energy of a system will allow 'other' electrons to penetrate the correlation hole of an electron, and so has the effect of reducing correlation. Therefore, exchange tends to be the more important effect in high density or high kinetic energy systems, it being a more 'hard-shell' effect. The total energy corrections beyond the Hartree model are termed exchange-correlation (xc) energy.

$$E^{NH} = T_S + V + E_H\left|n(r)\right| + E_{XC}\left|n(r)\right| \qquad (6.3)$$

where E_{xc} is the exchange-correlation energy.

6.2 Theory of ADF-BAND

The BAND density functional (DF) program performs electronic structure calculations on periodic systems. These can be bulk systems (3 dimensional), slabs (2 dimensional) or polymers (1 dimensional), and even molecules (0 dimensional).

The BAND density functional program uses the following formalism [8-10]

The Kohn-Sham theory of Density Functional method [11, 12] replaces the two-particle coulomb interactions $1/r_{12}$ between electrons by the sum of two one-particle operators. The first is the coulomb potential resulting from the average charge distribution. The second is the exchange-correlation (XC) potential that represents the exchange and correlation effects in an average way, and is a functional of the charge distribution.

Approximating non-relativistically, with motionless point nuclei, the Hamiltonian equation becomes

$$H\psi_n(\mathbf{k},\mathbf{r}) = \{T + V_C(\mathbf{r}) + V_{XC}(\mathbf{r})\}\psi_n(\mathbf{k},\mathbf{r}) = e_n(\mathbf{k})\psi_n(\mathbf{k},\mathbf{r})$$

T is the kinetic energy operator; $V_C(\mathbf{r})$ is the total coulomb potential, due to nuclear charges and the electron cloud; $V_{XC}(\mathbf{r})$ is the XC potential.

$\Psi_n(\mathbf{k},\mathbf{r})$ is a one-electron state with wave vector $\mathbf{k}$.

The solutions $\{e_n(\mathbf{k}), \Psi_n(\mathbf{k};\mathbf{r})\}$ vary continuously with $\mathbf{k}$ and thus form 'bands'; the subscript n, which enumerates the distinct solutions in $\mathbf{k}$, is called the band index.

$\mathbf{k}$ also serves as a symmetry label, donating the irreducible representations of the translation group corresponding to the Bravais lattice. The translation properties of $\mathbf{k}$ are expressed via Bloch's theorem

$$\psi_n(\mathbf{k},\mathbf{r}+\mathbf{R}) = e^{i\mathbf{k}\cdot\mathbf{R}}\psi_n(\mathbf{k},\mathbf{r})$$

where $\mathbf{R}$ is any point of the Bravais lattice. The states $\Psi_n(\mathbf{k};\mathbf{r})$ are computed as linear combinations of basis functions ϕ. These are chosen to belong to the same irreducible representations and are labeled accordingly: $\phi_i(\mathbf{k},\mathbf{r})$

the electronic charge density $\rho(\mathbf{r})$ is obtained by summation over all states with energy $e_n(\mathbf{k})$ below the Fermi energy e_F i.e. all occupied states. The summation includes the integration in k-space

$$\rho(\mathbf{r}) = \sum_n \int_{BZ} d\mathbf{k} |\psi_n(\mathbf{k},\mathbf{r})|^2 \theta(e_F - e_n(\mathbf{k}))$$

$\theta(x)$ is the Heaviside step function: θ=1 (x>0) or 0 (x<0).

The Fermi energy e_F is determined from the total electronic charge Q per unit cell

$$\int_{unitcell} \rho(\mathbf{r}) d\mathbf{r} = Q$$

The potentials $V_r(\mathbf{r})$ and $V_{XC}(\mathbf{r})$ are computed from the density $\rho(\mathbf{r})$ and depend on the solutions $\Psi_n(\mathbf{k},\mathbf{r})$. The self-consistent solutions are found by an iterative self-consistent field (SCF) procedure.

6.3 Computational Technique

A pseudo multi-point calculation was performed for H/Pd concentrations of 0, 0.125, 0.25, 0.375, 0.5, 0.625, 0.75, 0.875 and 1.0 (i.e. Pd, Pd_8H, Pd_4H, Pd_8H_3, Pd_2H, Pd_8H_5, Pd_4H_3, Pd_8H_7 and PdH). Using the same electronic starting configuration for each structure, the total formation energy was calculated for a range of lattice parameters about the experimentally determined value. The formation energy is calculated as the difference in energy between the starting electronic configuration for a collection of separate atoms and the final configuration as defined by that collection of atoms in the arrangement provided to the BAND program.

A second-order polynomial was fitted to the lowest points in each curve, and the minimum of this quadratic was taken as the minimum of the formation energy curve. This then provided a close approximation to the actual minimum-energy lattice spacing.

For reference (they are not referred to in this study), the position of some of the special points commonly used in FCC band diagrams are:

Γ = (0,0,0)

L = (½, ½, ½)

X = (0, 0, 1)

K = (¾, ¾, 0)

6.3.1 Unit Cells Used for Computations

Three basic unit cells were used for the DFT calculations. These three are based on the following palladium unit cells:

1. The single atom rhombohedral unit cell

This is the rhombohedral primitive unit cell of the face-centered-cubic structure. It is constructed with a lattice point located at the origin $(0,0,0)$ and uses primitive translation axes $\mathbf{a}_1, \mathbf{a}_2, \mathbf{a}_3$, which connect the origin lattice point with lattice points at the face center. For a FCC structure with cube side length, the primitive vectors are:

$$\mathbf{a}_1 = \frac{1}{2}a(\hat{\mathbf{x}}+\hat{\mathbf{y}}); \qquad \mathbf{a}_2 = \frac{1}{2}a(\hat{\mathbf{y}}+\hat{\mathbf{z}}); \qquad \mathbf{a}_3 = \frac{1}{2}a(\hat{z}+\hat{\mathbf{x}});$$

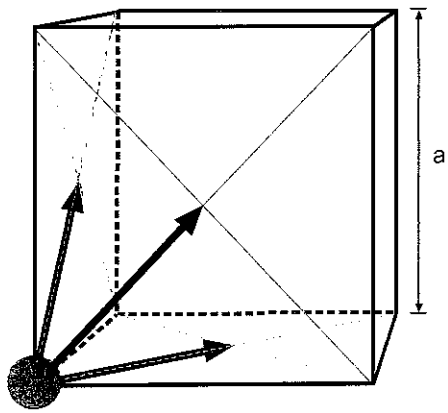

Figure 6.1 Primitive basis set for generating FCC structure. Single atom basis with rhombohedral translation axes.

$\hat{\mathbf{x}}$, $\hat{\mathbf{y}}$ and $\hat{\mathbf{z}}$ are the unit Cartesian vectors, and a is the cube-side length.

For pure palladium, a single Pd atom is placed at the origin. This is illustrated in figure 6.1. The octahedral site of this unit cell is at $\left(\frac{\mathbf{a}_1}{2},\frac{\mathbf{a}_2}{2},\frac{\mathbf{a}_3}{2}\right)$. The tetrahedral sites are at $\left(\frac{\mathbf{a}_1}{4},\frac{\mathbf{a}_2}{4},\frac{\mathbf{a}_3}{4}\right)$ and $\left(\frac{3\mathbf{a}_1}{4},\frac{3\mathbf{a}_2}{4},\frac{3\mathbf{a}_3}{4}\right)$. For stoichiometric palladium-hydride (PdH), an hydrogen atom is added to the octahedral site, forming the simple cubic NaCl structure. There is no point to adding further hydrogen or palladium atoms to this unit cell as only unnatural structures can result.

This is the highest symmetry unit cell for the FCC structure, and can be used by the ADF-BAND program as the least resource hungry method for computations on Pd and PdH.

2. A four atom cubic unit cell

This is a cubic unit cell with four lattice points. One lattice point is located at the origin, and one lattice point is located in the center of the three nearest cube faces to the origin, The translation vectors are in the direction of the Cartesian unit vectors i e

$\mathbf{a}_1 = a\hat{\mathbf{x}}; \qquad \mathbf{a}_2 = a\hat{\mathbf{y}}; \qquad \mathbf{a}_3 = a\hat{\mathbf{z}}$

This unit cell is illustrated in Fig 6.2.

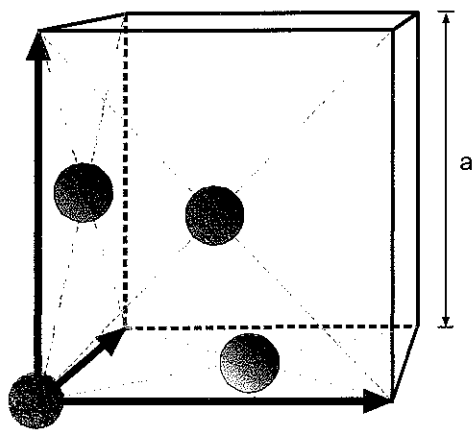

Fig 6.2: Cubic basis set for generating the FCC structure. Four atom basis with cubic translation axes.

With this unit cell it is possible to build the combinations Pd, Pd_4H, Pd_2H (as Pd_4H_2), Pd_4H_3 and PdH (as Pd_4H_4)

The octahedral sites in this structure are located at

$$\left(\frac{\mathbf{a}_1}{2},\frac{\mathbf{a}_2}{2},\frac{\mathbf{a}_3}{2}\right), \quad \left(\frac{\mathbf{a}_1}{2},\mathbf{0},\mathbf{0}\right), \quad \left(\mathbf{0},\frac{\mathbf{a}_2}{2},\mathbf{0}\right), \quad \left(\mathbf{0},\mathbf{0},\frac{\mathbf{a}_3}{2}\right)$$

The tetrahedral sites are located at

$$\left(\frac{\mathbf{a}_1}{4},\frac{\mathbf{a}_2}{4},\frac{\mathbf{a}_3}{4}\right), \quad \left(\frac{\mathbf{a}_1}{4},\frac{\mathbf{a}_2}{4},\frac{3\mathbf{a}_3}{4}\right), \quad \left(\frac{\mathbf{a}_1}{4},\frac{3\mathbf{a}_2}{4},\frac{\mathbf{a}_3}{4}\right), \quad \left(\frac{\mathbf{a}_1}{4},\frac{3\mathbf{a}_2}{4},\frac{3\mathbf{a}_3}{4}\right)$$

$$\left(\frac{3\mathbf{a}_1}{4},\frac{\mathbf{a}_2}{4},\frac{\mathbf{a}_3}{4}\right), \quad \left(\frac{3\mathbf{a}_1}{4},\frac{\mathbf{a}_2}{4},\frac{3\mathbf{a}_3}{4}\right), \quad \left(\frac{3\mathbf{a}_1}{4},\frac{3\mathbf{a}_2}{4},\frac{\mathbf{a}_3}{4}\right), \quad \left(\frac{3\mathbf{a}_1}{4},\frac{3\mathbf{a}_2}{4},\frac{3\mathbf{a}_3}{4}\right),$$

3. An eight atom rectilinear ("double-cubic") unit cell

This is a rectilinear unit cell with eight lattice points It can be thought of as a union of two four-atom cubic unit cells from 2 above. One lattice point is located at the origin of one of the

cubic cells $(0,0,0)$, along with the equivalent position in the second face-centered cube $\left(\frac{\mathbf{a}_1}{2},0,0\right)$. The other lattice points are at the equivalent positions in each cube as the 3 further lattice points in the four-atom cubic cell above at

$$\left(\frac{\mathbf{a}_1}{4},\frac{\mathbf{a}_2}{2},0\right),\quad \left(\frac{\mathbf{a}_1}{4},0,\frac{\mathbf{a}_3}{2}\right),\quad \left(0,\frac{\mathbf{a}_2}{2},\frac{\mathbf{a}_3}{2}\right),\quad \left(\frac{3\mathbf{a}_1}{4},\frac{\mathbf{a}_2}{2},0\right),\quad \left(\frac{3\mathbf{a}_1}{4},0,\frac{\mathbf{a}_3}{2}\right),\quad \left(\frac{\mathbf{a}_1}{2},\frac{\mathbf{a}_2}{2},\frac{\mathbf{a}_3}{2}\right)$$

With this unit cell we can generate the structures Pd, Pd_8H, Pd_4H (as Pd_8H_2), Pd_8H_3, Pd_2H (as Pd_8H_4), Pd_8H_5, Pd_4H_3 (as Pd_8H_6), Pd_8H_7 and PdH (as Pd_8H_8)

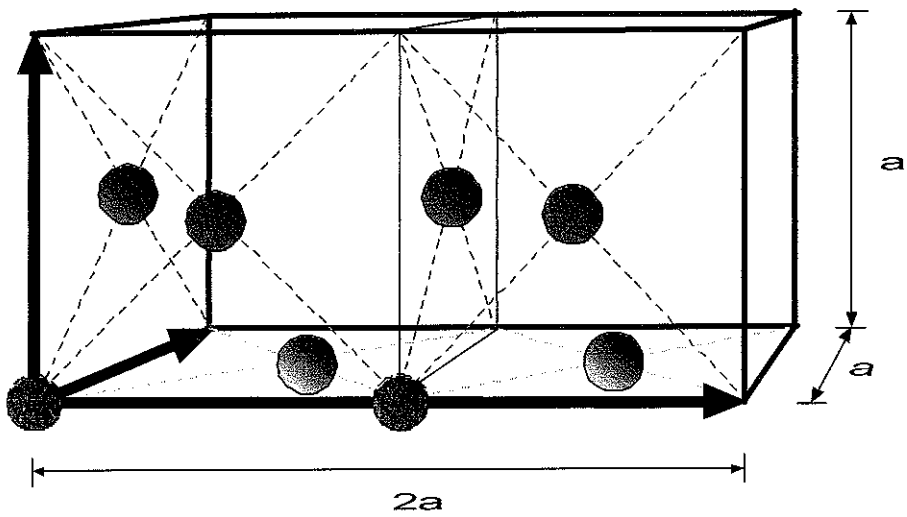

Figure 6.3 Double-cubic basis set for generating FCC structure. Eight atom basis with rectilinear translation axes.

There are then 8 octahedral sites and 16 tetrahedral sites in this structure.

The octahedral sites are

$$\left(\frac{\mathbf{a}_1}{4},\frac{\mathbf{a}_2}{2},\frac{\mathbf{a}_3}{2}\right),\quad \left(\frac{\mathbf{a}_1}{4},0,0\right),\quad \left(0,\frac{\mathbf{a}_2}{2},0\right),\quad \left(0,0,\frac{\mathbf{a}_3}{2}\right)$$

$$\left(\frac{3\mathbf{a}_1}{4},\frac{\mathbf{a}_2}{2},\frac{\mathbf{a}_3}{2}\right),\quad \left(\frac{3\mathbf{a}_1}{4},0,0\right),\quad \left(0,\frac{\mathbf{a}_2}{2},0\right),\quad \left(0,0,\frac{\mathbf{a}_3}{2}\right)$$

The tetrahedral sites are

$$\left(\frac{\mathbf{a}_1}{8},\frac{\mathbf{a}_2}{4},\frac{\mathbf{a}_3}{4}\right),\quad \left(\frac{\mathbf{a}_1}{8},\frac{\mathbf{a}_2}{4},\frac{3\mathbf{a}_3}{4}\right),\quad \left(\frac{\mathbf{a}_1}{8},\frac{3\mathbf{a}_2}{4},\frac{\mathbf{a}_3}{4}\right),\quad \left(\frac{\mathbf{a}_1}{8},\frac{3\mathbf{a}_2}{4},\frac{3\mathbf{a}_3}{4}\right)$$
$$\left(\frac{3\mathbf{a}_1}{8},\frac{\mathbf{a}_2}{4},\frac{\mathbf{a}_3}{4}\right),\quad \left(\frac{3\mathbf{a}_1}{8},\frac{\mathbf{a}_2}{4},\frac{3\mathbf{a}_3}{4}\right),\quad \left(\frac{3\mathbf{a}_1}{8},\frac{3\mathbf{a}_2}{4},\frac{\mathbf{a}_3}{4}\right),\quad \left(\frac{3\mathbf{a}_1}{8},\frac{3\mathbf{a}_2}{4},\frac{3\mathbf{a}_3}{4}\right),$$
$$\left(\frac{5\mathbf{a}_1}{8},\frac{\mathbf{a}_2}{4},\frac{\mathbf{a}_3}{4}\right),\quad \left(\frac{5\mathbf{a}_1}{8},\frac{\mathbf{a}_2}{4},\frac{3\mathbf{a}_3}{4}\right),\quad \left(\frac{5\mathbf{a}_1}{8},\frac{3\mathbf{a}_2}{4},\frac{\mathbf{a}_3}{4}\right),\quad \left(\frac{5\mathbf{a}_1}{8},\frac{3\mathbf{a}_2}{4},\frac{3\mathbf{a}_3}{4}\right)$$
$$\left(\frac{7\mathbf{a}_1}{8},\frac{\mathbf{a}_2}{4},\frac{\mathbf{a}_3}{4}\right),\quad \left(\frac{7\mathbf{a}_1}{8},\frac{\mathbf{a}_2}{4},\frac{3\mathbf{a}_3}{4}\right),\quad \left(\frac{7\mathbf{a}_1}{8},\frac{3\mathbf{a}_2}{4},\frac{\mathbf{a}_3}{4}\right),\quad \left(\frac{7\mathbf{a}_1}{8},\frac{3\mathbf{a}_2}{4},\frac{3\mathbf{a}_3}{4}\right)$$

6.3.2 Orbital Functions

The findings of [13] indicate that the electronic configuration of the palladium atoms impacts strongly on the width and position of the d-band. This fact, along with the enormous number of calculations required to cover all realistic hydrogen concentrations in palladium-hydride lead the current study to consider only *relative* band-structure changes. It is also widely accepted (see [14] and others) that DFT (the local approximation) can accurately predict lattice parameters, though often underestimating metallic elements by the order of 1%. DFT largely fails when estimating absolute energy values, especially when applied to d-band metals. Here the lattice parameter values were calculated as predicted. The free-atom palladium electronic structure chosen here was $4d^{10}$. The basis functions chosen for the palladium atoms were a mixture of spherically symmetric numerical (Herman-Skillman-type) functions for the occupied electronic states, Slater-type orbitals for the valence electronic states, and fit-functions for available states.

The calculations were spin-unrestricted and spin-orbit coupling was ignored. In the numeric orbitals shown below, a number following the electron-shell designation is the number of starting electrons in that shell. If no number follows, the shell is full. The shells were frozen (were not perturbed) up to and including 3S, but all states above this were used for the calculations. As numeric-orbitals are spherically symmetric, the squares of all *s*, *p* and *d* orbitals were used as fit-functions with $l=0$. The minimum and maximum range of atomic radii calculated for were 10^{-6} a.u. up to 100 a.u. using 2000 grid points.

For all calculations the atomic electronic configurations were as follows.

1. Palladium

Numeric orbitals:

```
1S
2S
2P
3S
3P
3D
4S
4P
4D 10.0
5S 0
```

Slater Functions

```
5S    1.4
5S    2.9
5d    2.3
```

Fit functions

```
9S          1.6000
9S          2.1800
9S          2.9700
8S          3.6400
8S          5.0500
8S          7.0000
7S          8.6400
7S         12.2400
6S         15.1800
6S         22.0600
5S         27.4800
4S         34.3300
3S         42.8100
2S         52.6000
1S         60.7000
9P          2.1300
9P          3.3100
```

8P	4.6600
7P	6.6500
6P	9.6300
5P	14.1800
4P	21.2800
3P	32.6000
2P	50.8500
8D	1.9500
8D	3.4200
7D	5.3800
6D	8.6500
5D	14.2700
4D	24.2400
3D	42.6500
7F	3.8500
6F	7.5200
5F	15.3100
4F	32.8000
7G	2.3000
6G	7.2200
5G	24.6000

2 Hydrogen

Numeric orbitals

1S

Slater Functions

2P	1.25
3D	2.5

Fit Functions

2S	1.50
4F	3.00
5G	4.00

ADF-BAND allows some control over the number of k-space points used for the calculation in reciprocal space, using the KSPACE variable. The available values are 3, 5, 7 and 9 and employ integration over the Brillioun Zone (BZ) using the quadratic tetrahedron method (all even values of KSPACE result in the inferior linear tetrahedron method). A KSPACE value of 1 uses only one k-space point, the origin.

The value assigned to KSPACE greatly influences the size and complexity of calculations. For configurations utilizing the primitive-single-atom-tetrahedral unit-cell or the four-atom-cubic unit-cell, it was possible to construct tractable calculations with KSPACE set to the maximum value of 9 i.e. configurations Pd, Pd_4H, Pd_2H (as Pd_4H_2), Pd_4H_3, PdH. When the eight-atom-"double-cubic" unit-cell was used i.e. Pd_8H, Pd_8H_3, Pd_8H_5 and Pd_8H_7 the maximum usable value of KSPACE was 3. Any larger values of KSPACE using the eight-atom unit-cell would cause a specific major intermediary file created by ADF-BAND, which BAND cannot split-up and distribute during parallelisation, to exceed the maximum *UNIX* file size of 2 gigabytes.

The Energy of Formation of a system is calculated with respect to the spherically symmetric, isolated, free atoms as specified in the startup configuration [9]. The experimentally determined configuration is not necessarily the optimal (i.e. most energetically profitable) starting point for a density functional, but was used for all calculations here. The configuration of the reference atoms does not affect the final self-consistent functional (SCF) density. This then justifies the procedure of choosing the same starting configurations for all atoms and only considering *relative* energies.

6.4 Calculated Lattice Parameters

The hydrogen to palladium concentrations considered were 0.0 (Pd), 0.125 (Pd_8H), 0.25 (Pd_4H), 0.375 (Pd_8H_3), 0.5 (Pd_2H), 0.625 (Pd_8H_5), 0.75 (Pd_4H_3), 0.875 (Pd_8H_7) and 1.0 (PdH). For each concentration, using the same configuration in each case, the Energy of Formation was calculated as the crystal structure was allowed to relax around the estimated minimum energy lattice parameter i.e. as extrapolated from the results of Chapter 4. These results were then plotted, and a 2nd order polynomial was fitted to the region around the estimated minimum. The minimum of this polynomial was then taken as the minimum energy lattice parameter.

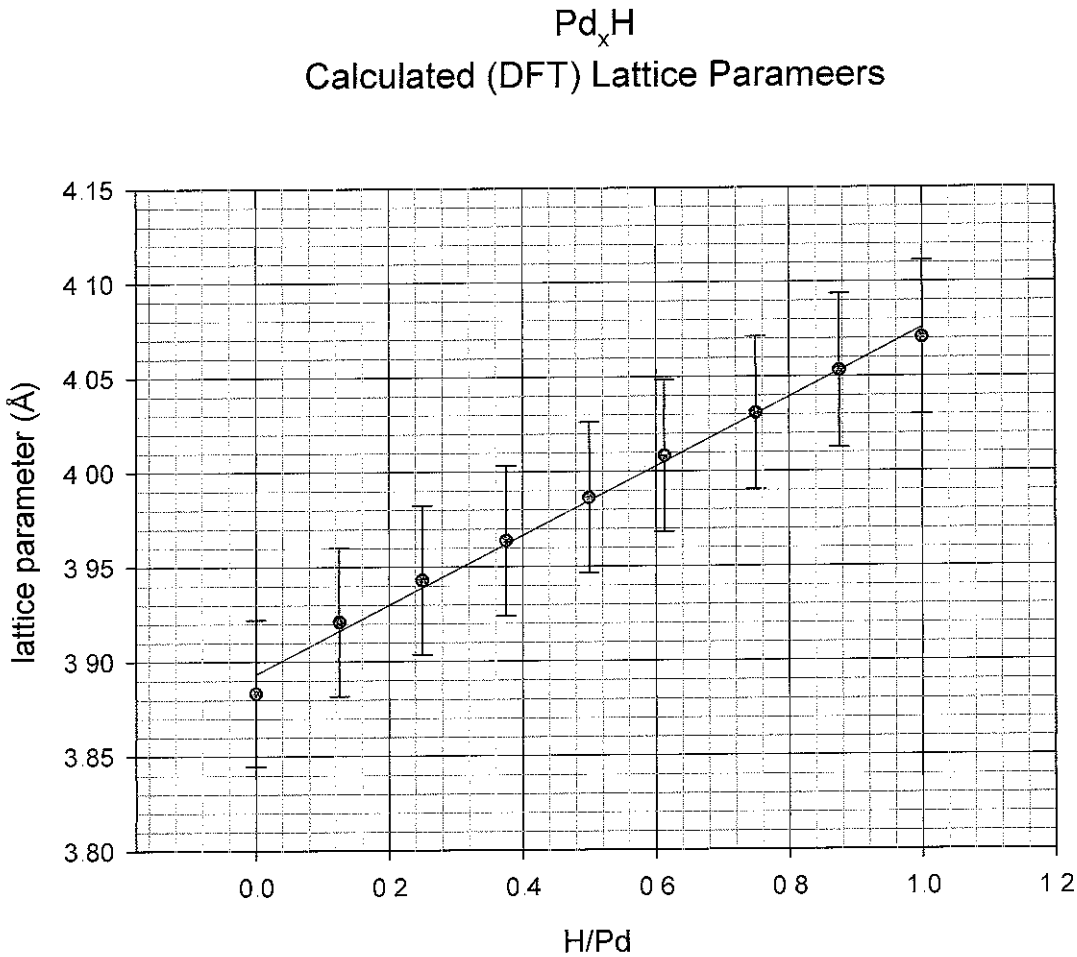

Figure 6.4: Calculated lattice parameters for Pd_xH. The red line is a linear regression through the data points. 1% error bars have been added.

Fig 6.4 plots the calculated lattice parameters against the hydrogen-to-palladium concentration of each configuration. Error bars of 1% have been added as the generally accepted error estimate [14]. The lattice parameters follow Vegard's Law (see Chapter 4). This shows the method's consistent results regardless of the unit-cell used (primitive, cubic, rectilinear).

The lattice parameter of the pure palladium calculation is not as consistent with the other points. Fig 6 5 shows the calculated points of Fig 6.4 plotted along with some of the, predominantly single-phase, measured lattice parameters from the experimental parts of this thesis (see Chapter 4). With the exception of the ISIS data, which has excellent overall agreement with the calculations, the experimental data agrees best with the calculations at low hydrogen concentrations. This could indicate that the Slater Functions and Fit Functions for elemental palladium need to be altered slightly when hydrogen is added

If the slope of the calculated lattice parameter curve stayed constant at the value it has between H/Pd = 0 and H/Pd = 0 125, there would be excellent agreement with the non-ISIS data up to H/Pd = 0 5

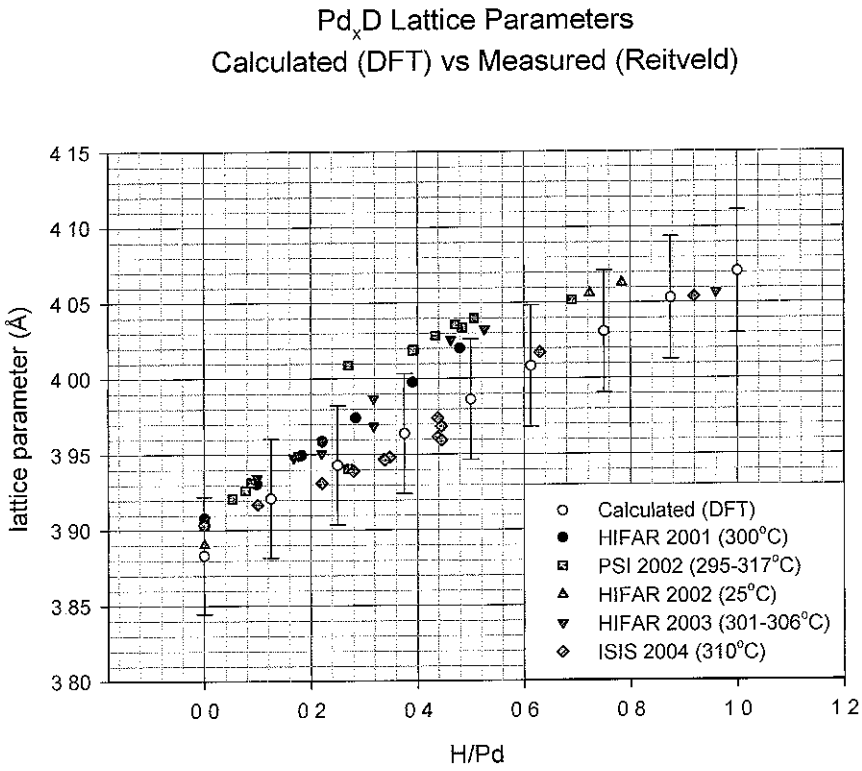

Figure 6 5: Calculated lattice parameters for Pd$_x$H compared to experimental results from this thesis

6.5 Octahedral and Tetrahedral Site Occupation

6.5.1 General Palladium-Hydrogen System Calculations

Fig 6 6 shows the results of a series of calculations designed to illuminate the preferred amount of hydrogen required in the tetrahedral sites, with the remainder occupying octahedral sites, for the range of hydrogen-to-palladium concentrations from 0 125 to stoichiometric PdH For each hydrogen concentration (i e. PdH_x where x=0 125, 0 25, 0 375, 0 5, 0.625, 0 75, 0.875, 1.0), a unit cell was constructed based on the rectilinear, "double-cubic", unit cell above, with all the attendant hydrogen atoms occupying octahedral sites in the palladium lattice at first. For each hydrogen-to-palladium concentration, the theoretical lattice parameters calculated in section 6 3 above, using all-octahedral models, were used The lattice was not relaxed for the repositioning of hydrogen atoms to the tetrahedral positions

In both α-phase and β-phase palladium the octahedral sites are occupied randomly by hydrogen atoms. With the relatively small unit-cells at our disposal here it is impossible to

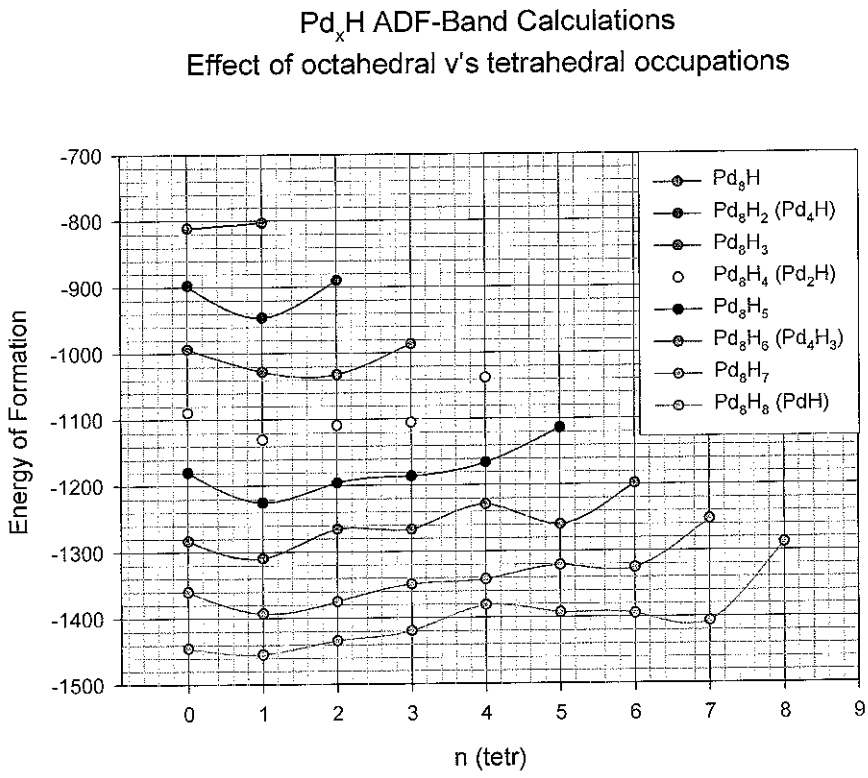

Figure 6 6: Palladium Hydride Energy of Formation – effect of moving hydrogen atoms from octahedral to tetrahedral sites The n (tetr) axis represents the number of hydrogen atoms of the total in each configuration occupying tetrahedral sites

accurately model such a random ordering, so a pseudo-random approximation was followed in that each added hydrogen atom was added to a different face-centered-cube than the previous Octahedral sites were also "paired" in constructing each octahedral-only configuration for increasing hydrogen concentrations, with every second hydrogen atom added to the rightmost cube of the double-cubic unit cell in the same octahedral site as the previous hydrogen atom was placed in the leftmost cube. So, Pd_8H had its octahedral hydrogen placed at position $\left(\frac{\mathbf{a}_1}{4}, \frac{\mathbf{a}_2}{2}, \frac{\mathbf{a}_3}{2}\right)$, Pd_8H_2 placed its two octahedral atoms at $\left(\frac{\mathbf{a}_1}{4}, \frac{\mathbf{a}_2}{2}, \frac{\mathbf{a}_3}{2}\right)$ and $\left(\frac{3\mathbf{a}_1}{4}, \frac{\mathbf{a}_2}{2}, \frac{\mathbf{a}_3}{2}\right)$ with a new octahedral site added for each pair of new increased concentrations. For each concentration, the total energy was calculated as each configuration moved its octahedral hydrogen to tetrahedral sites, one atom at a time, in a similar pair fashion as was followed in filling up the octahedral sites

The configurations of Fig 6.6 are shown in Table 6.1 , each bracketed configuration representing the site positions of the hydrogen atoms, O being octahedral, T being tetrahedral

Table 6.1: Unit-cell configurations used for palladium-hydrogen calculations

Formula	Unit-cell Configuration
Pd_8H:	(O), (T)
Pd_8H_2:	(OO), (TO), (TT)
Pd_8H_3:	(OOO), (TOO), (TTO), (TTT)
Pd_8H_4:	(OOOO), (TOOO), (TTOO), (TTTO), (TTTT)
Pd_8H_5:	(OOOOO), (TOOOO), (TTOOO), (TTTOO), (TTTTO), (TTTTT)
Pd_8H_6:	(OOOOOO), (TOOOOO), (TTOOOO), (TTTOOO), (TTTTOO), (TTTTTO), (TTTTTT)
Pd_8H_7:	(OOOOOOO), (TOOOOOO), (TTOOOOO), (TTTOOOO), (TTTTOOO), (TTTTTOO), (TTTTTTO), (TTTTTTT)
Pd_8H_8:	(OOOOOOOO), (TOOOOOOO), (TTOOOOOO), (TTTOOOOO), (TTTTOOOO), (TTTTTOOO), (TTTTTTOO), (TTTTTTTO), (TTTTTTTT)

The number of hydrogen atoms located at tetrahedral sites corresponds to values of the n (tetr) axis in Fig 6.6. It is apparent from these results that there is a preference for one hydrogen atom to occupy a tetrahedral site, except in the case of Pd_8H where the hydrogen atom prefers the octahedral position, and Pd_8H_3 where two of the hydrogen atoms will preferentially occupy the tetrahedral sites. It should be noted that these calculations were performed using a relatively low accuracy (KSPACE=3), though they are accurate enough to indicate general trends

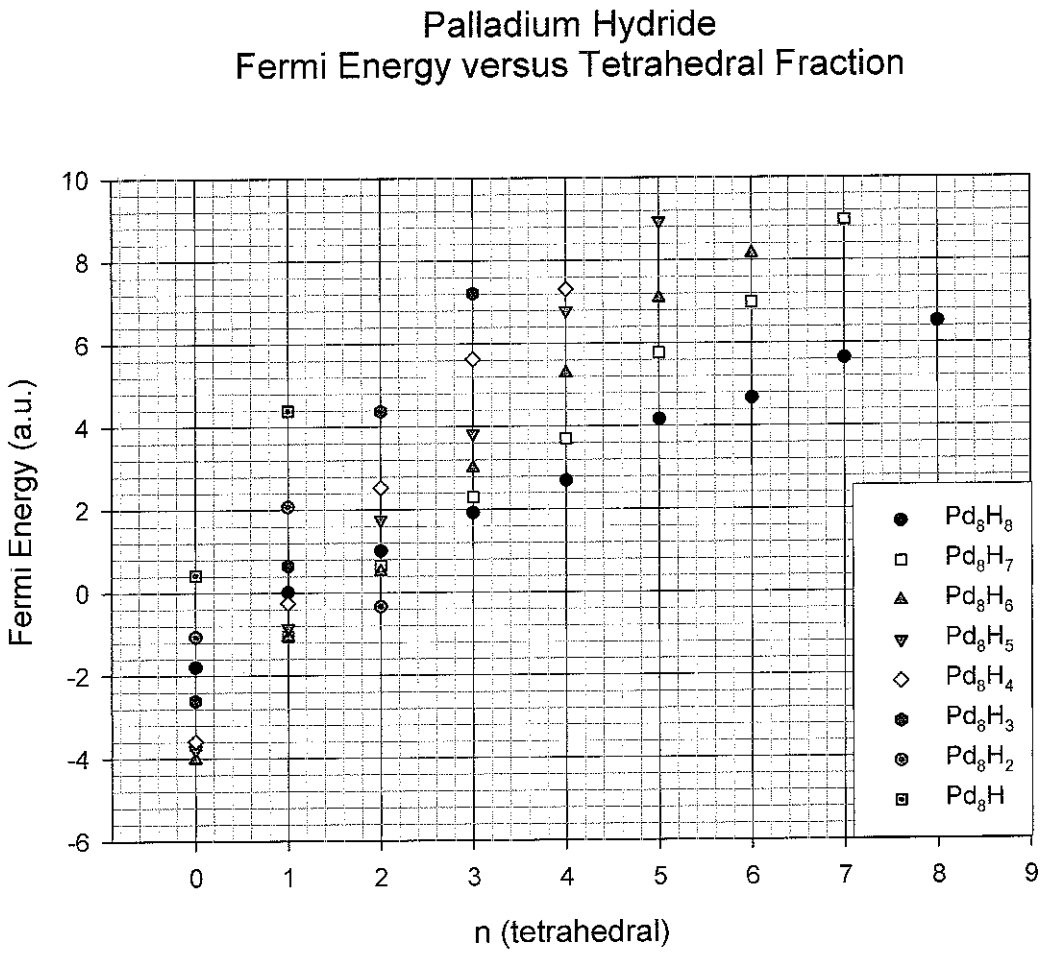

Figure 6 7: Palladium Hydride Fermi Energy – effect of moving hydrogen atoms from octahedral to tetrahedral sites. The n (tetr) axis represents the number of hydrogen atoms of the total in each configuration occupying tetrahedral sites

Fig 6 7 shows the Fermi Energy taken from the same calculations that produced Fig 6.6 Here we see a general trend of the Fermi surface increasing along with increased tetrahedral site occupation This is an indication that hydrogen atoms located in tetrahedral sites donate a larger part of their electron to the palladium band-structure than hydrogen atoms located in octahedral positions

An anomaly is observed in Fig 6 7 in the Fermi energy calculated for Pd_8H_2 with the configuration (TT) i.e with all hydrogen located in tetrahedral sites. It is thought that this may be an artifact of the computational method within BAND, as the calculations were checked and re-run several times, always producing the same result

6.5.2 Detailed Calculation of Pd_8H_3

Octahedral and tetrahedral site occupation in Pd_8H_3 was calculated independently with lattice relaxation from the octahedral only model allowed with movement of the hydrogen to tetrahedral sites The total energy of formation was calculated for each hydrogen configuration ((OOO), (TOO), (TTO), (TTT)) for a range of lattice constants from 3 8 Å to 4 4 Å. These results are shown in Fig 6 9

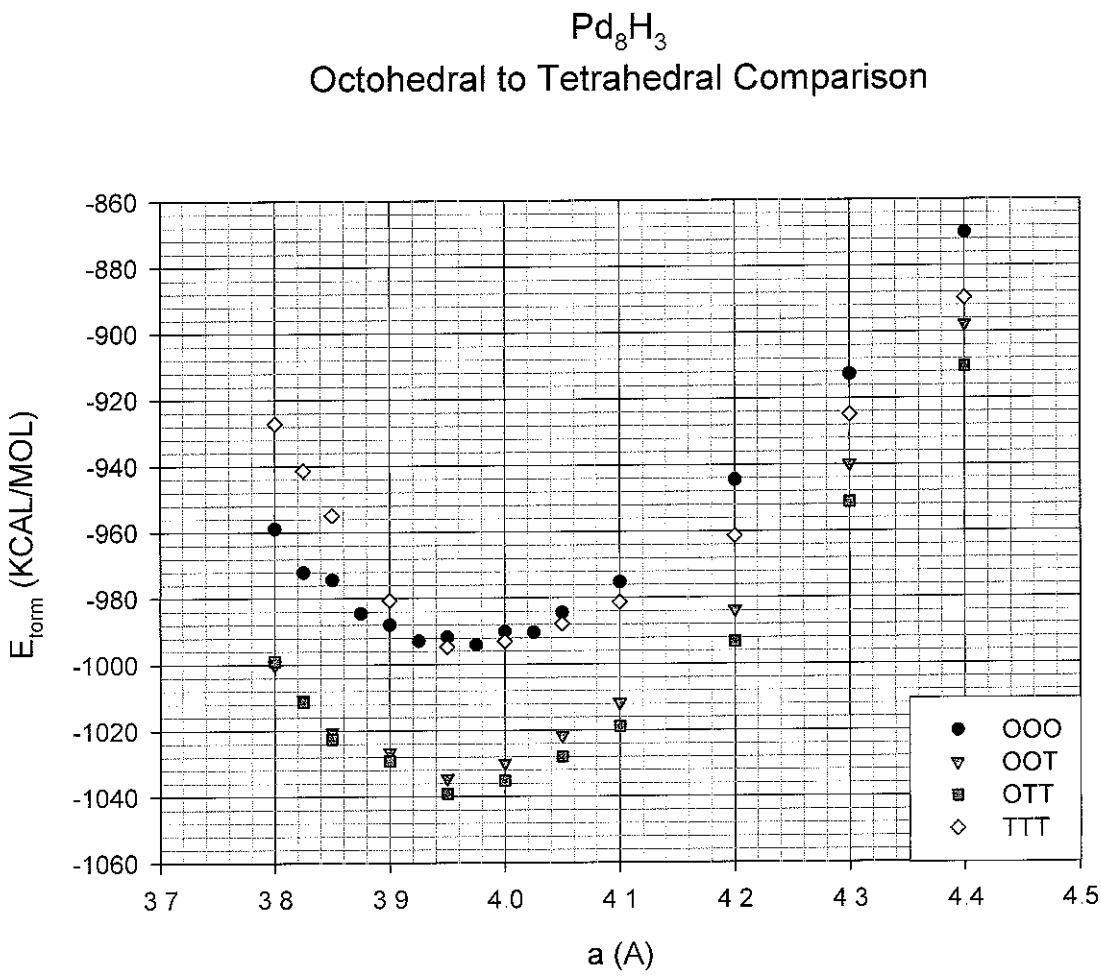

Fig 6 8 Pd_8H_3 Energy of Formation – octahedral/tetrahedral site occupation comparison

There is a clear preference for one or two hydrogen atoms in tetrahedral sites, just as in the results of Fig 6 6 for the un-relaxed lattice Note that for each Pd_8H_3 configuration, the lattice parametet corresponding to the minimum energy can be estimated from the plots in Fig 6 8

These are close enough to validate the calculations of Fig 6 6, which allowed no lattice relaxation from the octahedral-only model.

Some other features of Fig 6.8 are worth noting. The minimum energy lattice parameters of the "pure" configurations (all octahedral or all tetrahedral) are slightly larger than the minimum energy lattice parameters of the two "mixed" configurations ((TOO and (TTO)). At first glance, this would seem counter-intuitive. The space available for the hydrogen atoms in the tetrahedral site is smaller than that available in the octahedral site, so it would be assumed that increasing the tetrahedral site hydrogen content over the octahedral site content should have a increased effect on the lattice expansion.

The effect of increased tetrahedral site occupancy does behave intuitively in the case of "compressing" the Pd_8H_3. As the lattice parameter is reduced, the formation energy of the all-tetrahedral model rises most quickly. Examination of the two mixed configurations indicates that with decreasing lattice parameter, E_{form} begins to increase at a faster rate than for the all-octahedral configuration. There are also indications that E_{form} for the (TTO) model is increasing at a faster rate than the (TOO) model. This indicates that the occupied tetrahedral sites allow less compression of the palladium lattice. This is due to the fact that the distance between a tetrahedral hydrogen atom and its four nearest-neighbor palladium atoms is less than that between an octahedral hydrogen and its six nearest-neighbor palladium atoms.

The Bohr radius of a hydrogen atom is 0.529 Å and the tetrahedral hole has a radius ~0.31 Å. Given that the expansion of the palladium lattice with hydrogen absorption is at most 3-4%, this implies that where tetrahedral site occupation is concerned electronic effects are in evidence, with donation of some part of the hydrogen electron to the palladium band-structure.

6.5.3 Energy Profile of the Cube Diagonals

For this section particular notice should be paid to Fig 6.9. This figure shows a rectilinear "double-cubic" unit-cell (thick lines), drawn in perspective, surrounded by its 26 nearest-neighbor unit-cells (thin lines). The planes in the (010) direction have been color-coded increased clarity. This figure was used to understand the symmetry issues for different configurations of the Pd_8H_4 and Pd_8H_2 unit cells used in the DFT calculations on site occupation in Pd_2H and Pd_4H respectively.

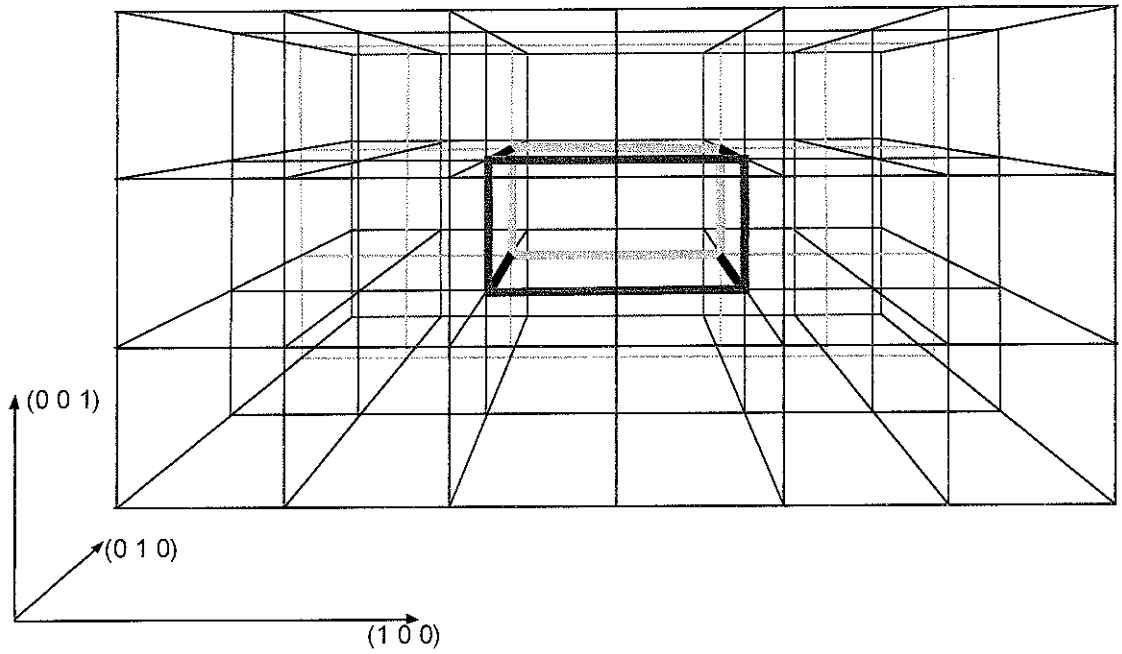

Fig 6.9: Nearest neighbour considerations for 8-atom rectilinear "double-cubic" unit cell

Pd_2H was chosen for the first study (Figs 6.10 - 6.14), as the results of section 5.5 in Chapter 5 show that the maximum total amount of tetrahedral site occupation near the critical temperature, occurs at a deuterium-to-palladium ratio close to 0.5 (see especially Fig 5.8). At this point the total tetrahedral sites occupied is in the range of 0.5 to 0.9 that of the total octahedral sites occupied. We construct eight-Pd-atom rectilinear unit-cells with one or two tetrahedrally located H atoms, and the remainder in octahedral positions (tet/oct = 0.33 or 0.5 respectively).

These calculations were constructed as follows. Using the 8-atom rectilinear palladium unit cell, various configurations of Pd_8H_4 were set up, always with two hydrogen atoms in each of

the two cubes in the unit-cell. Two or three of the hydrogen atoms were fixed in either octahedral or tetrahedral sites, and the remaining one or two hydrogen atoms were moved along particular cube diagonals while the formation and Fermi energies were calculated at regular intervals. The variable hydrogen atoms were moved from one the corners of a sub-unit-cell cube towards the diagonally opposite corner of the same cube. This passes the hydrogen atom through two tetrahedral sites and the octahedral site located in the center of the sub-unit cell cube.

Symmetry considerations mean that in a great deal of cases only positions in the first half of the diagonal need be calculated, as there will be positional symmetry of the hydrogen atoms about the octahedral site in the center of the cube when the nearest neighbor rectilinear cells are considered. Here then is the purpose of Fig 6.9

Figures 6.10 - 6.14 show the results of the calculations on Pd_2H.

There is an increase in the total energy as the mobile hydrogen atoms approach palladium atoms at the cube corners, or approach fixed hydrogen atoms at the octahedral site in the middle of a cube. The total energy of the mobile hydrogen atoms near tetrahedral sites is at a minimum, though the overall energy profile is quite flat.

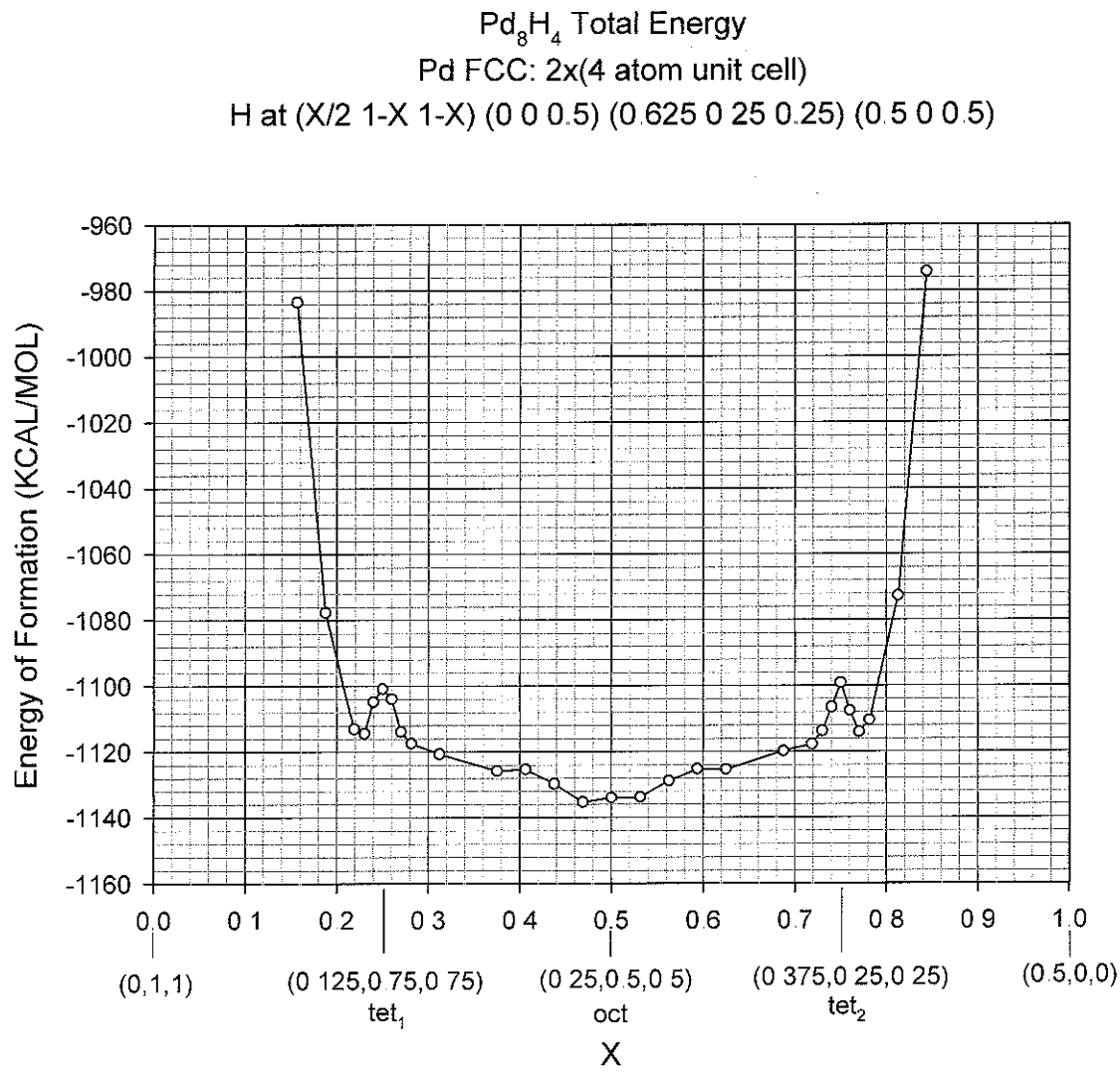

Fig 6.14: Energy of Formation: Pd_2H (Pd_8H_4): Unit cell (2x1x1) Two fixed octahedral H at (0 0 0 5) and (0.5 0 0.5) One fixed tetrahedral H at (0.625 0.25 0 25) Move single H along cube diagonal (X/2 1-X 1-X) varying X (0 0625 : 0 9375). This is the lowest symmetry operation considered. There is no symmetry around X=0.5.

The profile shown in Fig 6.14 was the lowest symmetry configuration considered. There is a minimum in the total energy very near the octahedral site for the mobile hydrogen atom. The peaks at the two tetrahedral positions are artifacts of the ADF-BAND computational technique.

This configuration reduces the symmetry of the systems as far as possible. Note the lack of symmetry in the total energy across the cube diagonal about the octahedral position. The two peaks at the tetrahedral positions, caused by interference with the symmetry operators of the

fixed tetrahedral hydrogen atom are an artifact of the calculation method. Notice that their behavior is slightly different, with tet_2, the tetrahedral site closer to the fixed tetrahedral hydrogen, being a sharper peak than tet_1. The tetrahedral position at (0.375,0.25,0.25) is 0.2500 units from the fixed tetrahedral position at (0.625,0.25,0.25), 0.8004 units from the octahedral position at (0,0,0.5) and 0.8750 units from the octahedral position a (0.,0,0.5). The tetrahedral position at (0.125,0.75,0.75) is 0.8660 units from the fixed tetrahedral position at (0.625,0.25,0.25), 0.5154 units from the octahedral position at (0,0,0.5) and 0.3750 units from the octahedral position a (0.,0,0.5)

Table 6.2 Distances, as a fraction of 'a' the cube side length, between some special positions in the Pd_8H_1 2x1x1 unit-cell

	Tetrahedral position 1 (0.125,0.75,0.75)	Tetrahedral position 2 (0.375,0.25,0.25)
Fixed tetrahedral position (0.625,0.25,0.25)	0.2500	0.8660
Fixed octahedral position 1 (0,0,0.5)	0.8004	0.5154
Fixed octahedral position 2 (0.5,0,0.5)	0.8750	0.3750

Pd_4H was also chosen for the next study (Figs 6.15 - 6.18) as the results of section 5.5 in Chapter 5 show that the total amount of tetrahedral site occupation at a deuterium concentration of 0.25 is very close to the total amount of octahedral site occupation. This implies that using the "double-cubic" rectilinear unit-cell, it is justifiable to model Pd_4H with one hydrogen atom at an octahedral site, and the second at a tetrahedral site in the other sub-unit cell cube

Note that peaks in the total formation energy often appear when the mobile hydrogen atom is placed at an equivalent position as occupied by the stationary hydrogen atom. This is an artifact of the computational methods used within ADF-BAND. So the mobile hydrogen, is free to move across the entire diagonal regardless of the location of the fixed hydrogen in the other sub-cube

6.6 Conclusions and Discussions

We have performed a series of computations on palladium-hydrogen using density functional theory techniques. This computational technique predicts the correct supercritical-like linear relationship between lattice parameter and hydrogen concentration within error. This is Vegard's Law as described in chapter 4. The agreement is with an *octahedral-only* structural model, with all hydrogen atom constrained to octahedral sites in the FCC palladium lattice. The technique of minimizing the lattice parameter/total energy data by simply fitting a 2^{nd}-order polynomial to the lowest few data points also proves sufficiently accurate for our purposes.

It is noted in section 6.4, from Fig 6.5, that the slope of the lattice parameter/concentration relationship over the interval from D/Pd=0 to 0.125 best fits most of the experimental data. The Numeric Orbitals, Slater Functions and Fit Functions specified for ADF-BAND in these calculations could be responsible for the misfit at higher hydrogen-to-metal ratios where the palladium band structure is highly perturbed. This misfit should be investigated, though this would not be a trivial matter.

Given the agreements between computations and experiment within error, we can be confident that the model used is an accurate reflection of the real palladium-hydrogen system, and can be used to investigate its other physical properties.

The study of Chapter 6 is restricted to considerations of relative energies only. The low number of k-space points possible for computations involving the rectilinear unit-cell (KSPACE=3) is suitable for calculating lattice parameters, so we can be confident that relative energy changes are suitable for conclusions to be made regarding other general trends.

The calculations provide more evidence for the occupation of palladium FCC tetrahedral sites by hydrogen. The unrelaxed lattice prefers one to two tetrahedral sites occupied with the remainder in octahedral sites for nearly all palladium-hydrogen concentrations.

In the final set of calculations involving the energy profiles of the cube diagonals, we find that in the case of Pd_2H hydrogen is free to move along the diagonal in the region of the

tetrahedral sites, with the octahedral site taken by other atoms. The configuration of Fig 6.15 shows that in this case the mobile hydrogen will occupy the octahedral site.

The cube diagonal calculations on Pd_4H employ a lone hydrogen in each of the sub-cubes in the rectilinear unit cell. The mobile hydrogen is free to move across the entire diagonal regardless of the location of the fixed hydrogen in the other sub-cube.

We have shown the usefulness of the DFT calculations by accurately calculating the lattice parameters associated with a range of palladium-hydrogen stoichiometries. Similar calculations have then been used to produce real evidence for tetrahedral site occupation of the palladium FCC lattice by hydrogen atoms. We have also shown that the hydrogen atoms possess some freedom to move about the cube diagonals.

1. Elasser, C., et al , Physica B, 1991. **40**(8): p. 217.
2. Elasser, C., et al , Phys. Rev. B, 1991. **44**(18): p. 10377.
3. Elasser, C , et al., J. Phys.: Condens. Matter, 1992. **4**: p. 5207.
4. Elasser, C , et al., Phys. Rev. B, 1994. **50**(8): p. 515.
5. Ho, K M., et al., J. Phys : Condens. Matter, 1992. **4**: p. 5189.
6. Krimmel, H., et al , J. Phys : Condens. Matter, 1994. **6**: p. 7679-7704.
7. Dobson, J F., *Electron Density Functional Theory*. International Journal of Modern Physics B, 1999. **13**(5 & 6): p. 511-523.
8. SCM, *BAND: a Fortran program for structure calculations*
9. SCM, *BAND Users Guide*.
10. SCM, *ADF Users Guide*.
11. Hohenburg and W. Kohn, 1964.
12. Kohn, W. and L J. Sham, Physical Review, 1965. **140**(4): p. A1133.
13. Mueller, F M., et al., Physical Review B, 1970. **1**(12): p. 4617-4635.
14. Perdew, J P., et al , Physical Review B, 1992. **46**(11): p. 6671-6687.

Summary

The palladium-hydrogen system has been studied experimentally using in-situ neutron diffraction techniques and theoretically using Density Functional Theory. Despite the fact that the palladium-hydrogen system is the oldest and most thoroughly studied of all the metal-hydrides we have still managed to gain some new insights into its processes. This was the first in-depth neutron-diffraction study of the region around the palladium-hydrogen critical temperature, referred to here as the peri-critical region.

We have identified some crucial thermodynamic differences between bulk forms of palladium, in this case sheet palladium and finely divided palladium. The differences are apparent in the shape of pressure-composition isotherms available in the literature, and in the value of the critical temperature, here determined via diffraction.

The use of neutron powder diffraction techniques has shown that the thermodynamic critical temperature cannot accurately be predicted by the disappearance of hysteresis in the pressure-composition isotherms. A more reliable measurement of the critical temperature is made by observing the disappearance of the two-phase lattice parameters via diffraction. This is an issue which should be more fully explored in the future, with a thorough diffraction study, using a high resolution instrument, to determine the exact critical temperature via the lattice parameters.

As an insight into improving the storage capacity of all metal hydrides, the issue of tetrahedral occupation in palladium-hydrogen is crucial. There are twice as many tetrahedral sites available in the FCC lattice as octahedral sites, so preferential occupation of all of the tetrahedral sites could conceivably double the storage capacity of palladium. An understanding of tetrahedral versus octahedral occupation in palladium may provide a basis for the study of similar situations in other metals, where more numerous, though at first sight energetically less favourable sites may also be available.

In three separate experiments, two performed as part of this thesis and another performed elsewhere but analysed here using the same technique, consistent evidence for partial occupancy of tetrahedral sites was found. Tetrahedral occupancy of the palladium FCC lattice by deuterium near and above the critical temperature has therefore been shown to be real

The Density Functional Theory (DFT) calculations provided evidence to support tetrahedral occupation of hydrogen in palladium. We can be sure our computational technique is solid since DFT accurately predicts the single-phase lattice parameter/concentration relationship (a form of Vegard's Law) The calculations show that hydrogen does prefer to occupy some of the available tetrahedral sites They also show that the hydrogen atoms are free to move about the cube diagonal due to a relatively flat energy profile.

We have demonstrated that new and useful science can be gained from the study of palladium-hydrogen, even though it is a system long-thought to have been fully explored. The fact that it is a very simple system makes it ideal to study via computational techniques using modest computer resources. It also makes it useful to study via modern, high-resolution micro-probe techniques such as neutron diffraction, where its simplicity allows the study of fundamental, and at times subtle, science

References

Ali, J. K , E. J. Newson, et al. (1994). Journal of Membrane Science **89**: 171-184.

Amandussen, H., L -G. Ekedahl, et al (2000). Applied Surface Science **153**: 259-267

Anderson, I. (1994). in Neuron Scattering from Hydrogen in Metals (Proceedings of the Second Zuoz Summer School on Neutron Scattering). A Furrer. Singapore, World Scientific: 142-167.

Anderson, I S., C. J. Carlile, et al. (1978). J. Phys C: Solid State Phys. 11: L381.

Anderson, I S., D. K Ross, et al (1978). Phys Lett. 68A(2): 249.

Baranowski, B., S Majchrzak, et al. (1971) Journal of Physics F: Metal Physics **1**: 258-261

Beg, M. M. and D. K Ross (1970) J. Phys C: Solid State Phys. 3: 2487.

Bennington, S M , M. J. Benham, et al. (1990). Journal of Electroanalytic Chemistry **281**: 323-330

Bergsma, J and J. A. Goedkoop (1960) Physica **26**: 744-750.

Blaschko, O., P. Fratzl, et al (1981). Phys. Rev. B **24**: 277.

Blaschko, O., R. Klemencic, et al (1978). Solid State Communications **27**: 1149

Blaschko, O , R. Klemencic, et al. (1979). J Phys. FL Metal Phys. **9**(6): L113.

Blaschko, O., R. Klemencic, et al. (1980) Acta Cryst. A 36: 605.

Chen, W C. and B J. Heuser (2000). **312**: 176-180.

Davis, W. D. (1954) Knolls Atomic Power Laboratory Report No. 1227

Davis, W. D (1955). Knolls Atomic Power Laboratory Report Number 1375.

Dobson, J. F (1999). International Journal of Modern Physics B **13**(5 & 6): 511-523

Elasser, C , M Fahnle, et al. (1991). Physica B **40**(8): 217.

Elasser, C., M. Fahnle, et al (1994). Phys. Rev. B **50**(8): 515

Elasser, C , K. M. Ho, et al. (1991). Phys Rev B **44**(18): 10377.

Elasser, C., K M. Ho, et al. (1992). J Phys : Condens. Matter **4**: 5207.

Ellis, T. E., C. B. Satterthwaite, et al (1979) Phys. Rev. Lett. **42**(2): 456.

Entin, I R., V A Somenkov, et al. (1974). Sov. Phys. Solid State **15**: 1840.

Feenstra, F and R. Griesen (1986) Solid State Communications **59**(12): 905-908.

Feenstra, R., D G. d. Groot, et al (1984). Journal of the Less-Common Metals **104**: 43-49.

Ferguson, G A , A. J Schindler, et al. (1965). Physical Review A **137**: 483

Frieske, H. Thesis (1972) Munster.

Frieske, H and E Wicke (1973). Ber. Bunsenges. Physik Chem. **77**: 50.

Fukai, Y. (1993). The Metal-Hydrogen System. Berlin, Springer-Verlag

Gray, E M. (1991) Unpublished.

Gray, E. M. (2000). Private Communication. Brisbane.

Hemmes, H., A. Driessen, et al (1986) Journal of Physics C: Solid State Physics **19**: 3571-3585.

Ho, K M., C. Elasser, et al. (1992) J. Phys : Condens Matter **4**: 5189

Hohenburg and W. Kohn (1964).

Hunter, B A. (1998) Commission on Powder Diffraction Newsletter **20**: 21

Jacobs, J. K and F. D Manchester (1976). J Less-Common Met. **49**: 67.

Kennedy, S. J., E Wu, et al (1995) J. Phys : Condens Matter **7**: L33.

King, H. W and F D Manchester (1978). Journal of Physics F **8**: 15.

Kisi, E. Private Communication (2004).

Kohn, W and L. J. Sham (1965). Physical Review **140**(4): A1133

Krimmel, H , L Schimmele, et al. (1994) J. Phys.: Condens. Matter **6**: 7679-7704.

Kruger, F. and G Geh (1933). Ann. Phys. **16**: 174.

Lawson, A. C., J. W. Conant, et al (1992). J Alloys Comp. **183**: 174

Lewis, F A. (1967). The Palladium/Hydrogen System. London, Academic Press Inc

Maeland, A. J and T. R. P. j. Gibbs (1961). Journal of Physical Chemistry **65**: 1270.

McKeehan, L. W (1923). Physical Review **21**: 334-342

McLennan, K. G and E M. Gray (2004). Measurement Science and Technology **15**: 211-215.

Michels, A., W. de Graaff, et al (1959). Physica **25**: 25-42.

Mills, R. L , D. H. Liebenberg, et al. (1978) The Journal of Chemical Physics **68**: 2663

Mills, R L , D. H Liebenberg, et al (1977). The Journal of Chemical Physics **66**(7): 3076-3084

Morreale, D. D., M. V. Ciocco, et al. (2004). Journal of Membrane Science **241**: 219-224

Mueller, F. M., A J Freeman, et al. (1970) Physical Review B **1**(12): 4617-4635.

Mueller, M. H., T O. Brun, et al (1979). AIP Conf. Proc. **53**: 391.

Mueller, M H , J. Faber, et al. (1975). Acta Cryst. A **31**: S99.

Mukhopdyay, R., B. A Dasannacharya, et al. (1990) Solid State Communications **75**(4): 359-362.

Nace, D. M. and J G. Ason (1957). Journal of the American Chemical Society **79**: 3623.

Nelin, G. (1971) Phys. Stat. Sol. **45**: 527

Nernst, G H (1963). Thesis, Munster

Ogden, J. M. (2002). Physics Today April 2002: 69-75.

Perdew, J. P., J. A. Chevary, et al. (1992). Physical Review B **46**(11): 6671-6687.

Pitt, M. P. (2003). Thesis, Brisbane, Griffith University

Pitt, M. P. and E. Mac. A. Gray (2003). Europhysics Letters **64**(3): 344-350.

Roa, F. and J. D. Way (2005). Applied Surface Science **240**: 85-104

Rosenhall, G. (1933). Ann. Phys. **18**: 150.

Ross, D. K., M. W. McKergow, et al. (1991). J. Alloys Comp. **172-174**: 169.

Rybalko, V. F., A. N. Morozov, et al. (2001). Physics Letters A **287**: 175-182.

Schirber, J. E. and B. Morosin (1975). Physical Review B **12**(1): 117-118.

SCM BAND Users Guide.

SCM "BAND: a Fortran program for structure calculations."

SCM ADF Users Guide

Suleiman, M., J. Faupel, et al. (2005). Journal of Alloys and Compounds In Press

Tang, I., S.-l. Guo, et al. (2005). Materials Science Forum **275-279**: 2485-2488.

Tkacz, M. and A. Litwiniuk (2002). Journal of Alloys and Compounds **330-332**: 89-92.

Vegard, L. (1921). Phys. **17**: 5

Vegard, L. (1928). Z. Kristallogr. **67**: 239.

Wang, D., T. B. Flanagan, et al. (2004). Journal of Alloys and Compounds **372**: 158-164.

Wicke, E. and J. Blaurock (1987). Journal of the Less-Common Metals **130**: 351-363.

Wicke, E. and H. Brodowsky (1978). in Hydrogen in Metals II: Application-Oriented Properties. G. Alefeld and J. Volkl. Berlin, Springer-Verlag. 29: 81

Wicke, E. and G. H. Nernst (1964). Ber. Bunsenges. Physik. Chem. **68**: 224.

Worsham Jr., J. E., M. K. Wilkinson, et al. (1957). J. Phys. Chem. Solids **3**: 303-310.

Wu, E., S. J. Kennedy, et al. (1996). J. Phys. Condens. Matter. **8**: 2807.

Wu, E., S. J. Kennedy, et al. (1995). J. Alloys Comp. **231**: 108.

Yamada, M. (1922). Philosophical Magazine **45**(265): 241-243